MSUCP-32
June 1980

A SURVEY OF BEAM DYNAMICS PRIOR TO EXTRACTION IN THE K-500 CYCLOTRON AT M.S.U.

E. Fabrici and F.G. Resmini
Cyclotron Laboratory, Michigan State University
East Lansing, MI 48824

ABSTRACT

This paper presents a detailed study of the accelerated beams dynamics, prior to extraction, for the K-500 cyclotron under construction at M.S.U. The results, for a number of representative beams, indicate that adequate turn to turn separation can be achieved, while keeping distortions to a substantially negligible level. The presence of the $\nu_R+2\nu_Z=3$ resonance, and its effect in limiting the cyclotron dynamic range is also discussed.

1. Introduction

The present analysis of beam dynamics for the M.S.U. K-500 superconducting cyclotron has the main goal of establishing the conditions under which proper turn to turn separation can be achieved at extraction radius, while preserving the necessary beam quality in phase space.

Excitation of the $\nu_{R=1}$ resonance, as in conventional A.V.F. cyclotrons, looks the only viable method. Consequently, the amplitude and phase of the field first harmonic needed to excite the resonance, and of those inherently present in the field because of the magnetic channels used in the extraction, have been carefully investigated.

This study was carried out, using very realistic and perfectly isochronized magnetic fields, on a set of eight representative ions spanning the entire cyclotron operating range both in terms of the charge to mass ratio and the magnetic field level. A brief review of the calculation methods and the general properties of the magnetic field is given below.

2. General Outline and calculations methods

We shall use these notations:

-Z/A = charge to mass ratio (electron charge/amu) of the accelerated particles

-B_o = nominal center field value, usually in kgauss, for which isochronism has been calculated

-T/A = ions energy in MeV/n

The customary notation ν_R and ν_Z shall be used for the radial and axial focusing frequencies respectively, while the R.F.

frequency is denoted by ν_{RF}. Its harmonic number with respect to the particle orbital frequency is h.

It is useful to recall some features of the pole tip geometry of the machine. Hills and valleys, following a spiral law with 1/13 (rad/inch) constant, are shown in fig. 1 together with the extraction scheme. The azimuthal scale is also shown, in order to help relating the azimuth values, given in the following, to the actual pole geometry. More details on the latter are given in [1] and [2].

All the calculations reported here use very realistic magnetic field maps, i.e. obtained from measured data by the methods described in detail in [2].

The average field is properly isochronized with a least squares fitting procedure. The latter uses both the main coils and trim coils, and takes into account the actual variation, as a function of the main coils currents, of the field generated by the iron configuration. The azimuthal step of a map is 1^{o}, thus allowing Runge-Kutta integration at 2^{o} intervals. The radial step size is .5".

Equilibrium orbit properties are derived via the equilibrium orbit code, on field maps having threefold-120^{o} symmetry. Accelerated orbits are tracked with the code SPIRAL-GAP[3], generally on 360^{o} maps. The latter are obtained by superposing to the 120^{o} maps the calculated perturbing effects of the hardware needed for extraction. It will be recalled[4] and it is also shown in Fig. 1 that the extraction system employs several passive magnetic channels, made with iron bars, whose effects, mostly in terms of the field 1^{st} and 2^{nd} harmonics,

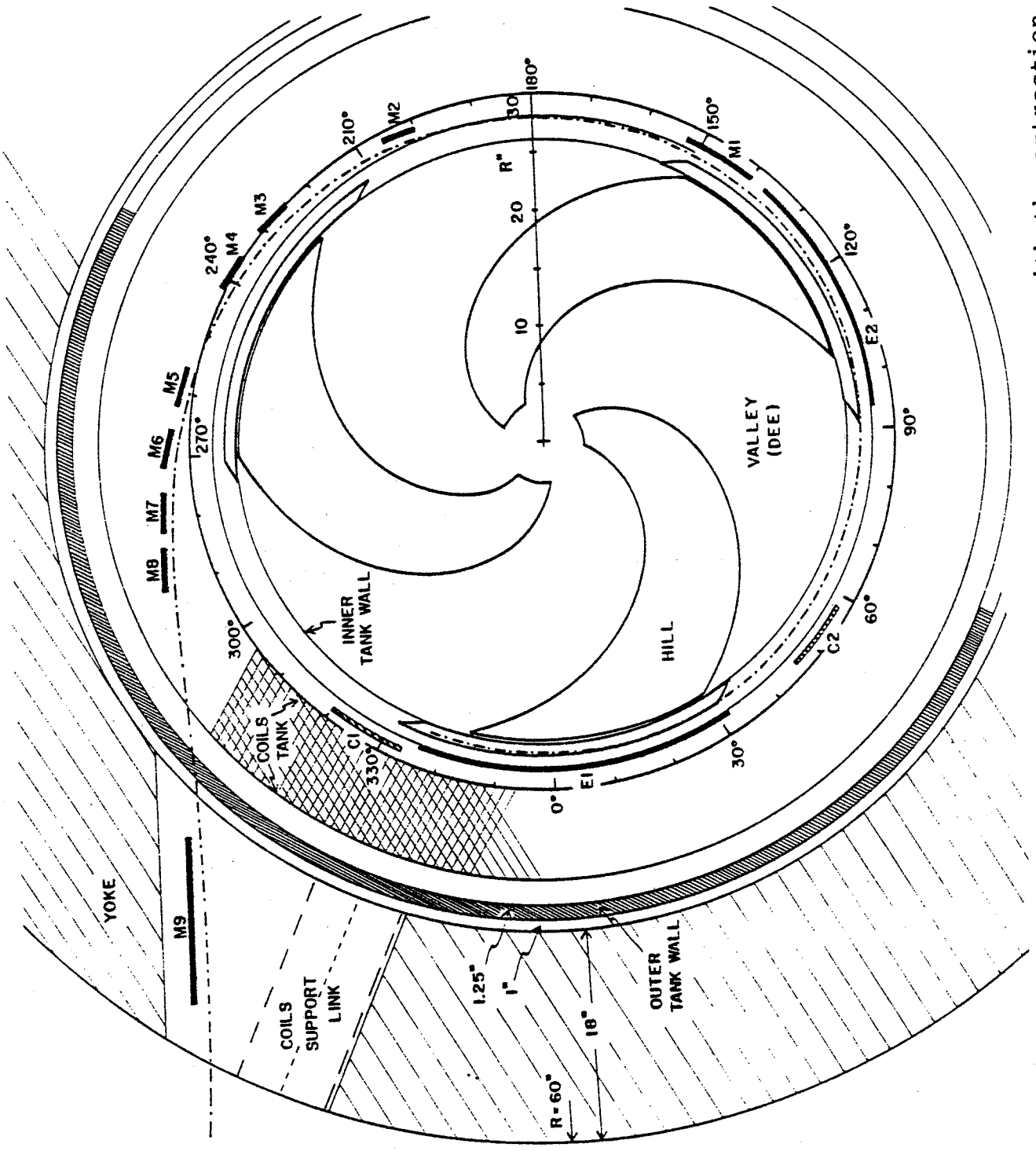

FIG. 1. Median plane geometry of the K-500 cyclotron together with the extraction scheme.

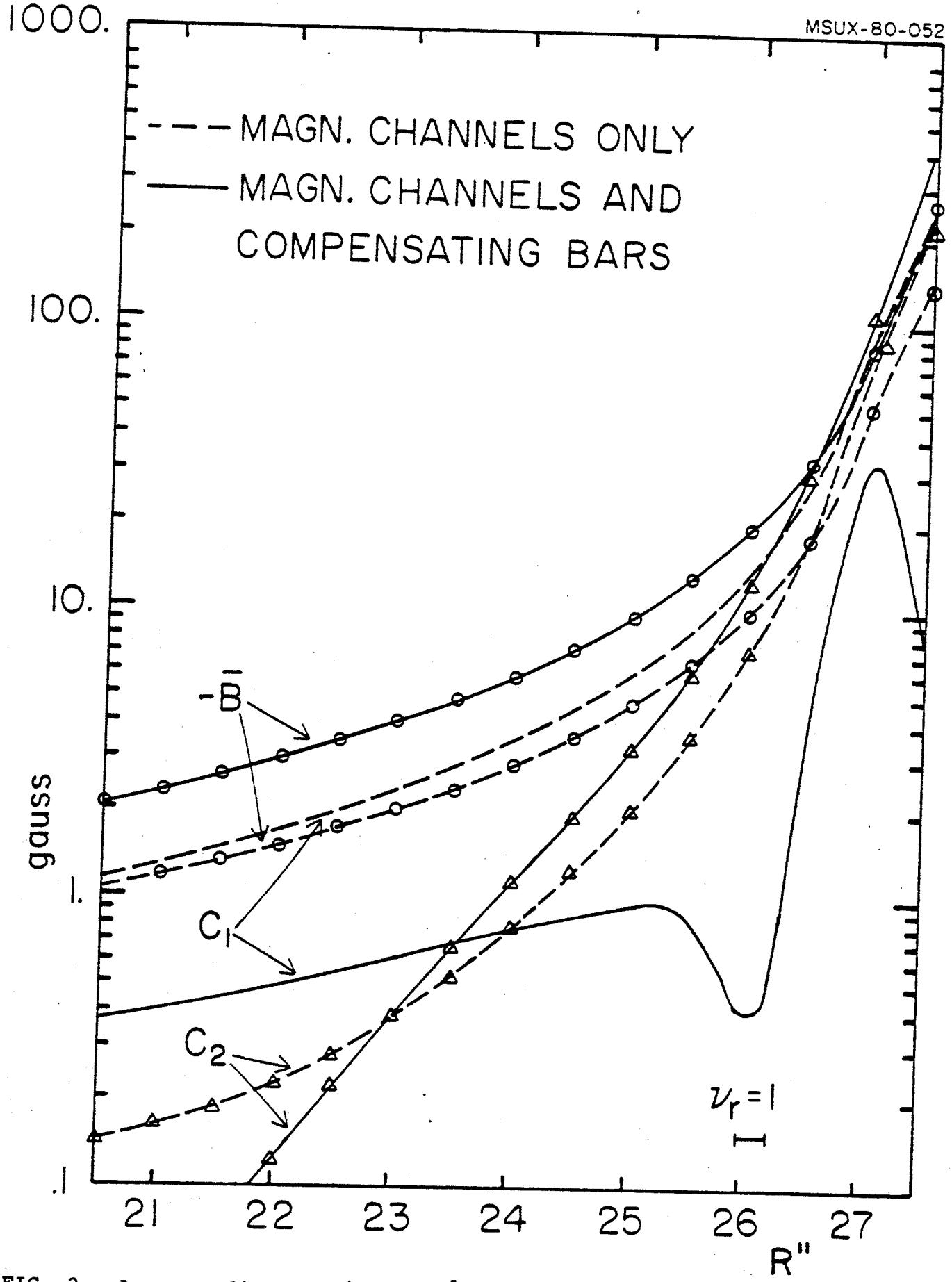

FIG. 2. Average field, 1st and 2nd harmonics produced by the magnetic channels and the compensating bars.

have to be compensated. The final design of the system is described in detail in [5] and differs in some aspects from the one presented in [4]. The uncompensated average field, first harmonic C_1, and second harmonic C_2, produced by the final set of magnetic channels are shown by dashed lines in Fig. 2. The compensated ones (see [5] for hardware details) are indicated by solid lines. The compensated fields are then added to the 120^{o}-symmetric maps to provide a realistic 360^{o} map. Measured 1^{st} and 2^{nd} harmonics, as produced by imperfections in the poles etc.[6] are also added. The present calculations are therefore self-consistent.

As stated above, a first harmonic field component will be used in proximity of the ν_R=1 resonance to excite the radial precession which allows the optimization of the turn to turn separation at the deflector entry. In our case, adjustment of the amplitude and phase of the 1^{st} harmonic will be achieved through the last (13^{th}) trim coil. We recall that the trim coils are wrapped around each of the three 46^{o} wide hills and therefore independent excitation of the three sections will allow said control. The form factor of one of these 46" wide sections is presented in Fig. 3 both for the average field and the first three harmonics for 100 A current. It will be noted that these contributions peak between 25.5" to 26.5" in radius, which is where ν_R=1 occurs, and decrease rapidly on either side. It was checked that the actual form factor influences the orbits much as if the first harmonics had a constant value over the ν_R=1 region. For this reason a radially flat first harmonic has been used in the present calculations.

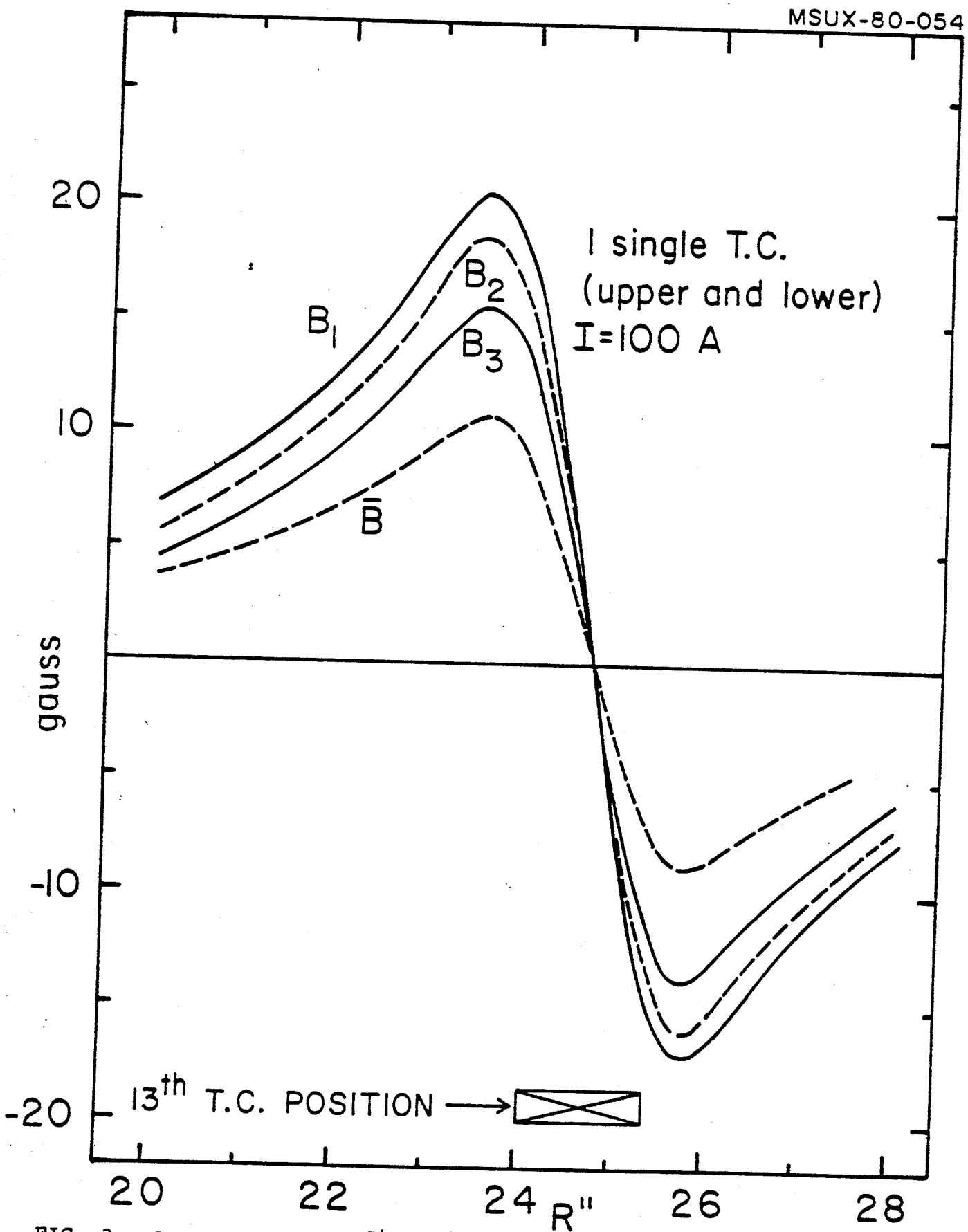

FIG. 3. Average field, 1st, 2nd and 3rd harmonics for 100. A in the 13th trim coil.

2. Equilibrium orbit properties

The K-500 operating diagram in the (B_o, Z/A) plane is shown in Fig. 4, as bounded by the bending limit K=500, i.e. 50 kgauss field at extraction, focusing limit K_{FOC}=160 [$T/A \leq K_{FOC} \cdot Z/A$], Z/A=.5 and B_o=30 kgauss limits. We shall comment the latter two limits in the following. Also shown in Fig. 4 are constant T/A lines. As reported earlier[7] the machine should operate both as a stand-alone cyclotron with internal ion source, and as injector for the planned K-800 cyclotron. In the latter mode the required energies/nucleon are between 7 MeV/n and .2 MeV/n, these being the highest energy for light ions and the lowest energy for heavy ions[8]. The corresponding area in the (B_o,Z/A) plane covers the Z/A range up to .15, higher Z/A are to be used in the stand-alone mode only.

In order to investigate the beam dynamics features we have chosen a set of eight representative ions on the countour of the (B_o,Z/A) diagram, as shown by dots in Fig. 4. The corresponding values of Z/A, B_o, T/A, etc. are also listed in Table I. In the following we shall normally identify these ions by their $Z/A/B_o$ numbers.

The ions energy as a function of the R.F. frequency is plotted in Fig. 5 for the various harmonic modes. The stand-alone and injector bands are also indicated.

Of key importance for the beam dynamics near the extraction radius, and henceforth for the design of an extraction system, is the behaviour of ν_R in this region. This is shown, for six ions, in Fig. 6 as a function of the equilibrium orbit

MSUX-80-162

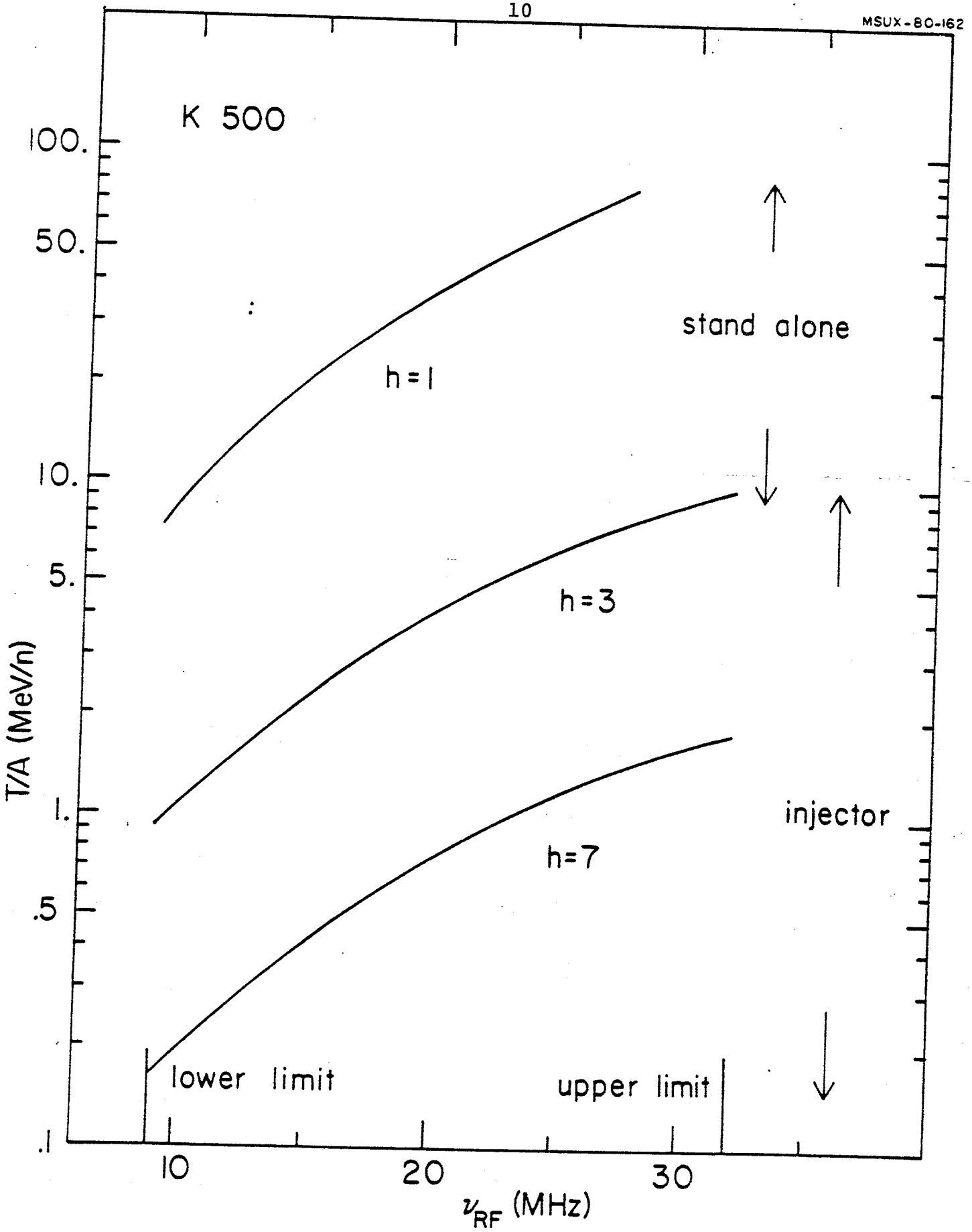

FIG. 5. T/A as function of ν_{RF} for various harmonic modes.

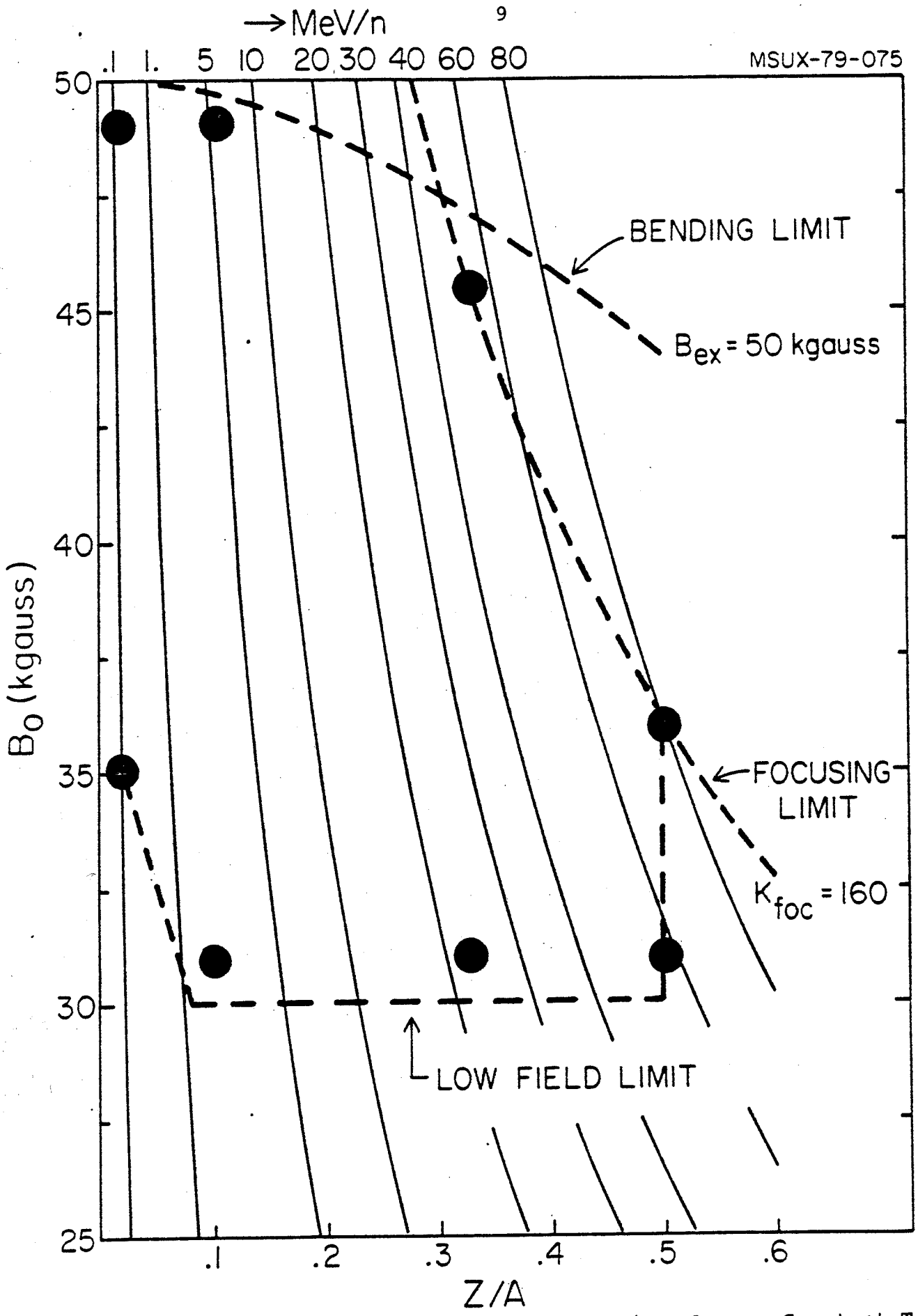

FIG. 4. K-500 operating diagram in the (B_o,Z/A) plane. Constant T/A lines are also shown. Dots indicate representative ions for this study.

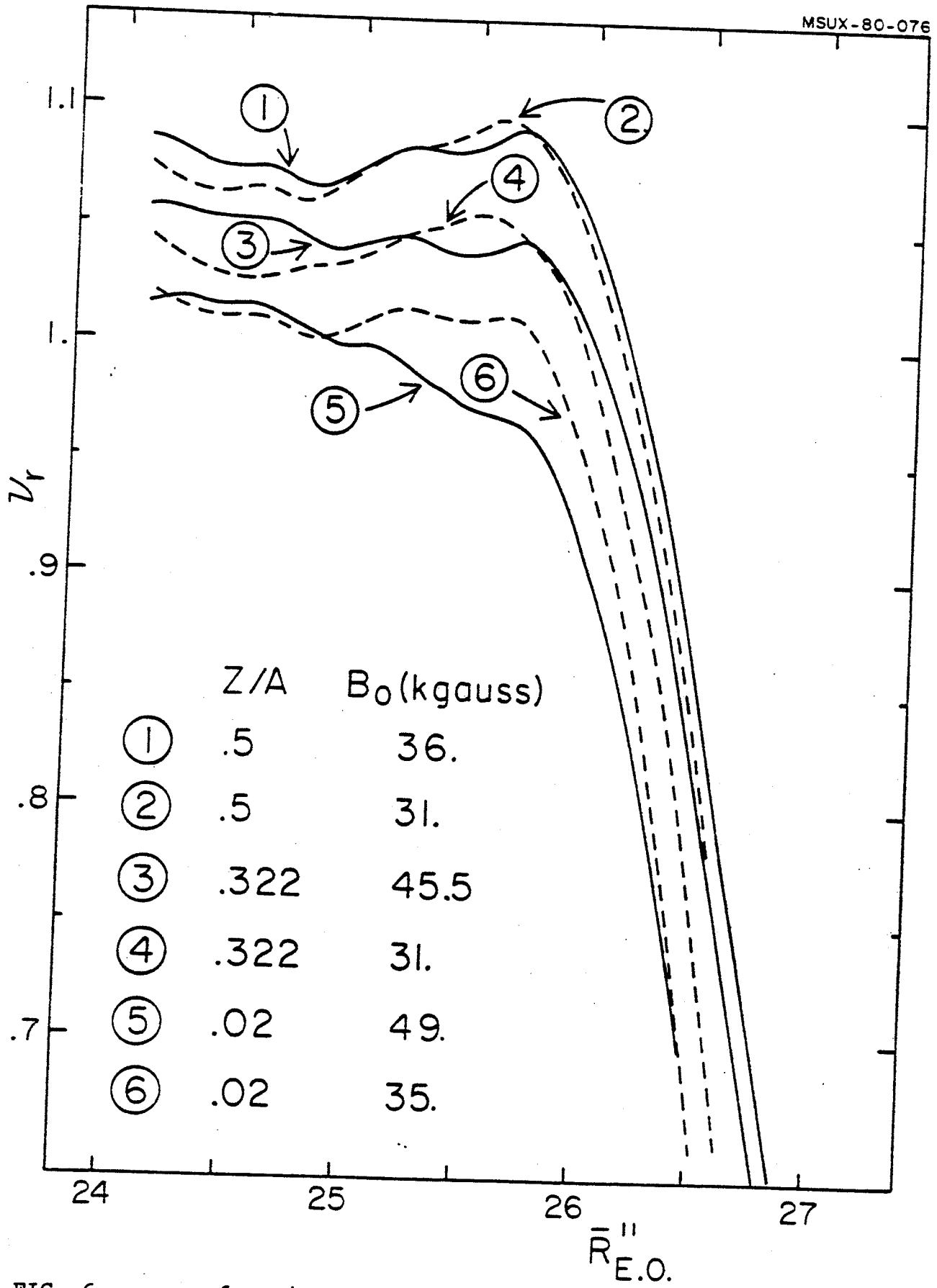

FIG. 6. ν_R as function of the equilibrium orbit radius for the listed ions.

Table I. Representative ions data

Z/A	B_o (kG)	T/A_{extr} (MeV/n)	P_{extr} (inches)	ν_{RF} (Mhz)	h	V_{dee} (kV)	N_{turns}
.5	36.0	79.41	28.65	27.64	1	100.	530
.5	31.0	56.03	27.80	23.80	1	100.	375
.322	45.5	49.81	27.67	22.50	1	100.	516
.322	31.0	22.15	26.88	15.33	1	100.	230
.1	49.0	5.15	26.28	22.57	3	70.	123
.1	31.0	2.05	26.20	14.28	3	97.	36
.02	49.0	.203	26.06	10.53	7	85.5	40
.02	35.0	.103	26.04	7.52	7	62.	29

radius. Any given ν_R value below ν_R=1 occurs at a different radius depending upon the type of particle and field. Typically the radius at which a given ν_R is reached moves inward in going from the most relativistic particles to the least relativistic ones. The effect, as explained in [2], is due to the main coils field which shifts inward at the different excitations needed for isochronizing the average field. The total radial span at, say, ν_R=0.8, which is a typical value for extraction, is .4". The slopes of the ν_R vs R curves also indicate that at fixed R the corresponding range of ν_R would be very high, like from 0.7 to 0.9. These circumstances over which one has practically no control, suggest that a radially movable extraction system may be more suitable if proper optimization of the deflected beams is to be achieved over the whole operating range.

The (ν_R, ν_Z) plots for the Z/A=.5 ions (fully stripped light ions) are shown in Fig. 7 for B_o values of 36 and 31 kguass, and for an energy range of a few MeV/n prior to extraction. The main feature is the appearance of the $\nu_R + 2\nu_Z = 3$ resonance, described in [8]. As shown by Fig. 7, the resonance is approached at higher values of ν_R the lower the magnetic field, the physical reason being the increase in ν_Z due to the $\frac{1}{B^2}$ flutter increase. This resonance cannot be approached, much less crossed, in a cyclotron since a very large axial beam blowup occurs. This actually starts a few turns before the crossing, as shown for the 0.5/31 ion in Fig. 8. Only a perfectly centered beam could theoretically cross the resonance without suffering a devastating blow-up, but this is hardly the case after the passage of the $\nu_R=1$ resonance and prior to extraction, where off-centering is required to enhance the turn to turn separation.

The lower limit of about 30 kguass on B_o is set precisely because of this problem. As shown in Fig. 9 for three different ions, at the same B_o field of 31 kguass, the operating (ν_R, ν_Z) plots tend to coincide, i.e. the flutter increase effect and the corresponding ν_Z increase in overwhelming. At this field level and as shown by Fig. 9, extraction must then take place at $\nu_R \sim 0.85$-0.9 which means both a more difficult extraction and, because of the slope of the ν_R vs R curves, more internal radii. No extensive studies have been carried out so far to precisely determine the lowest operational B_o field for each particle. The data now available indicate that operation and extraction at 25 kgauss is nearly impossible and is somewhat

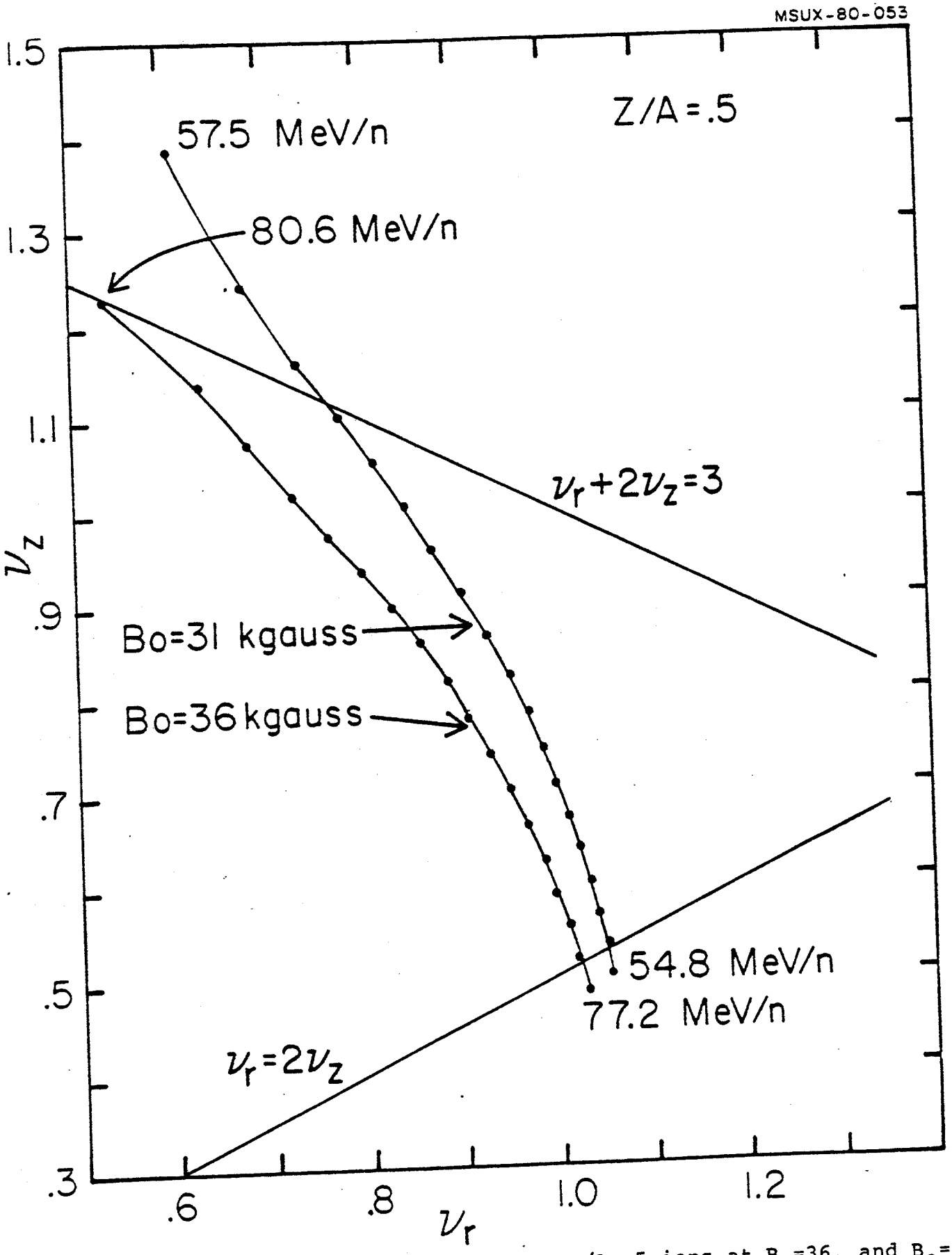

FIG. 7. Operating (ν_z,ν_r) plots for the Z/A=.5 ions at B_o=36. and B_o=31. kguass.

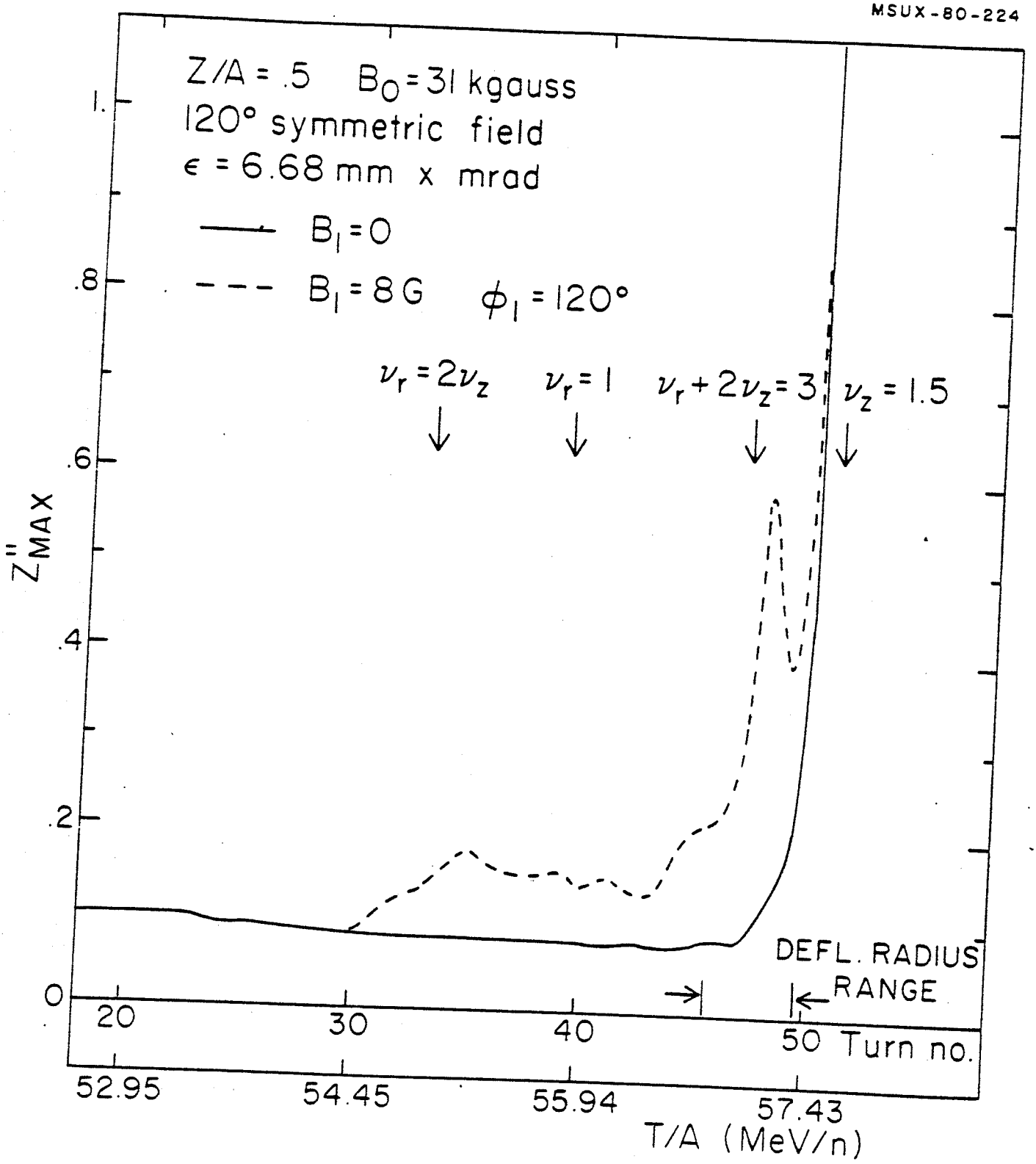

FIG. 8. Axial beam blow-up near the crossing of the $\nu_R + 2\nu_Z = 3$ resonance for a centered and off centered beam.

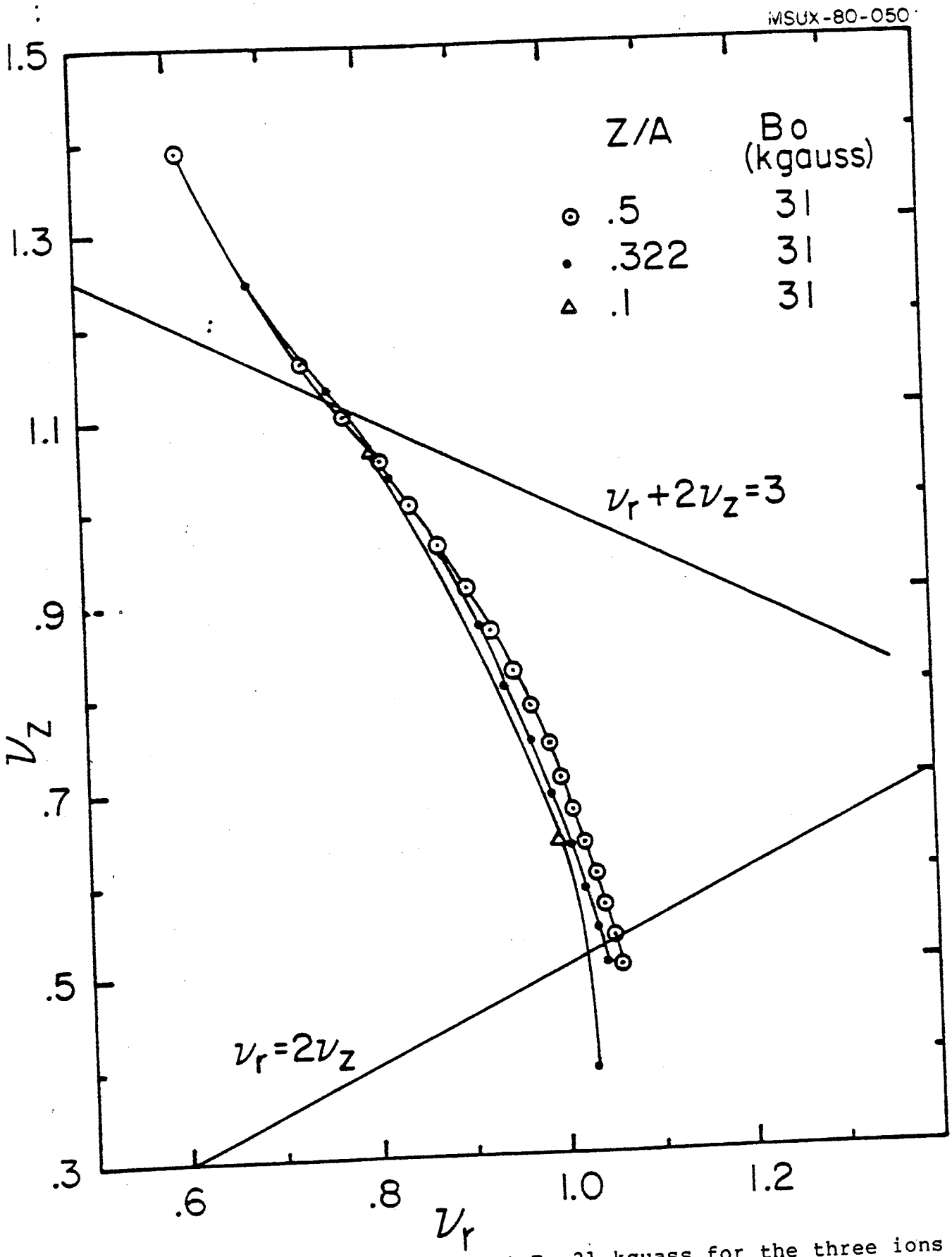

FIG. 9. Operating (ν_Z,ν_R) plots at B_o=31 kguass for the three ions listed.

marginal at 28 kgauss. The present choice of 30 kgauss is therefore a conservative one.

The possibility of using the K-500 cyclotron for accelerating ions with Z/A >.5, i.e. $^3He^{++}$ (Z/A=.667) and protons has been explored. The (ν_R,ν_Z) plots for three different $^3He^{++}$ energies at B_o=25, 27, and 28 kguass are shown in Fig. 10. The highest energy shown, 96 MeV/n, corresponds to a K_{FOC}=145 and this beam hits the resonance at a ν_R value of $\sim$0.85. However, extraction of such a highly relativistic particle is impossible with the present scheme since it requires electric fields in the deflectors higher than 150 kV/cm. At lower energies, the resonance hits the beam at ν_R close to 1, so that again extraction becomes difficult, because of the inner extraction radius. In summary, it could be that $^3He^{++}$ may be accelerated and extracted, but just over an extremely narrow range of energies. This will be fully investigated for the final field configuration. Acceleration and extraction of protons is instead out of question for the same reasons as in the $^3He^{++}$ case, the resonance being hit at very inner radii.

The discussion of accelerated orbits will therefore be confined to the eight representative ions listed in Table I.

3. Accelerated orbits

The process of determining the proper conditions for an accelerated beam to clear the deflector septum and be successfully extracted is obviously an iterative one, and mostly

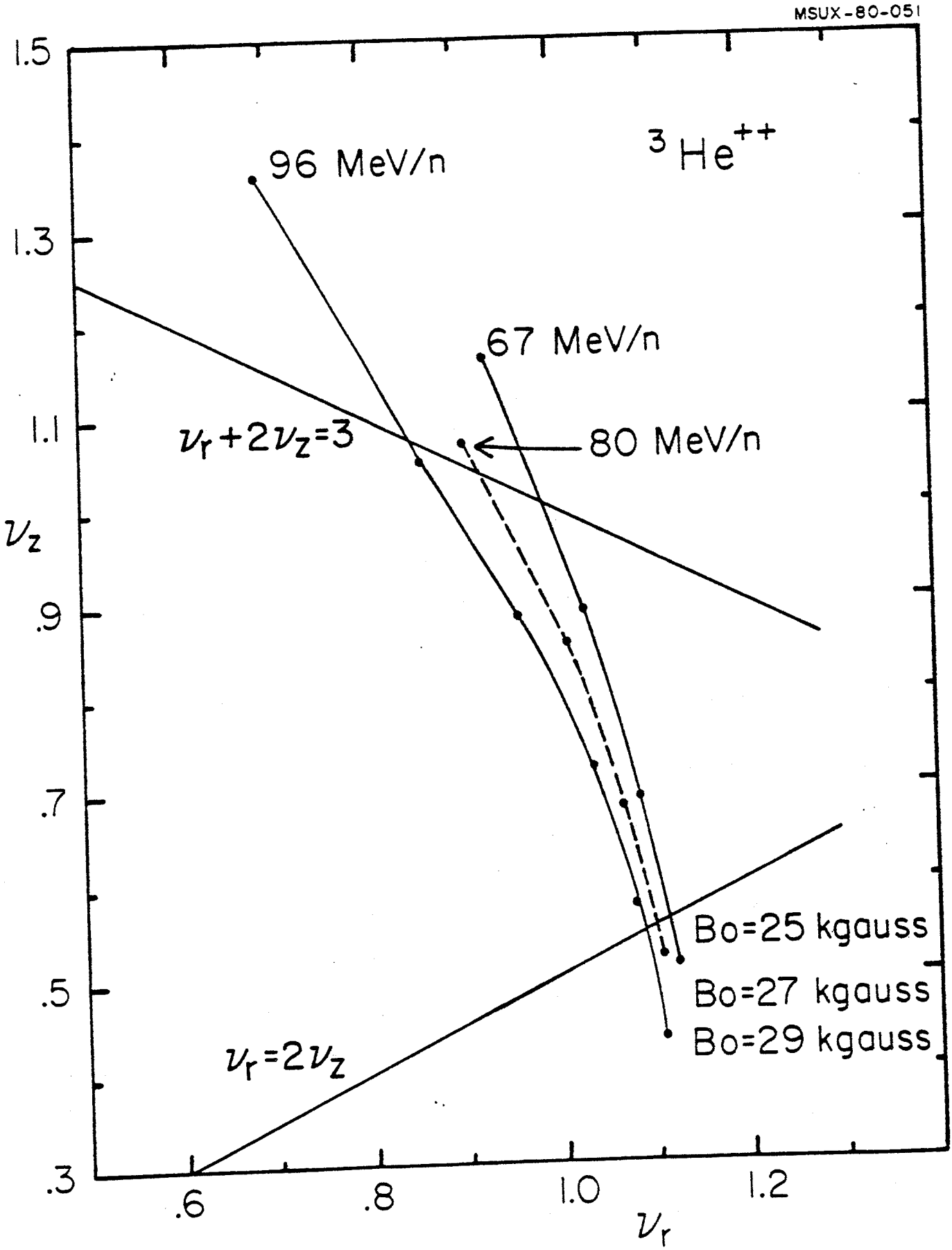

FIG. 10. Operating (ν_Z,ν_R) plots for $^3He^{++}$ at three different center field levels.

a tedious one too. We shall only discuss here the final results and for this purpose we recall some aspects of the extraction scheme, more details being given in [5].

The system consists of two electrostatic deflectors, positioned in two consecutive hills, followed by eight passive channels as schematically shown in Fig. 1. The two deflectors span the azimuthal range from $\theta=-23^{o}$ to $\theta=+32^{o}$, and from $\theta=94^{o}$ to $\theta=137^{o}$ respectively. Henceforth the entrance of the first deflector is at $\theta=-23^{o}$. All following phase plots are given at $\theta=-30^{o}$, which is however very close to the actual deflector entrance.

A number of iterations have shown that for the most relativistic particles to be extracted with reasonable electric fields on the deflectors, i.e. less than 140 kV/cm over 8 mm gaps, the orbit should have at $\theta=-30^{o}$ a radius of at least 26.5"-26.6". The said radius is only 1.5" inside from the outer iron boundary[1,2] but nevertheless it can be reached with an acceptable phase slip, as will be seen later.

Even at the high fields of a superconducting cyclotron a first harmonics of small amplitude at $\nu_R=1$ will generate the radial precession needed to clear the septum of the deflector. An example of this is shown for the 0.5/36 (80 MeV/n) ion, in Fig. 11 and 12. The radii of successive turns for the central ray are displayed, at $\theta=-30^{o}$, for a variable 1^{st} harmonics amplitude and fixed phase of $\phi_1=60^{o}$, Fig. 11, or for a variable phase and fixed amplitude of $B_1=1$ guass, Fig. 12. Other details are given in self-explanatory way on the figures

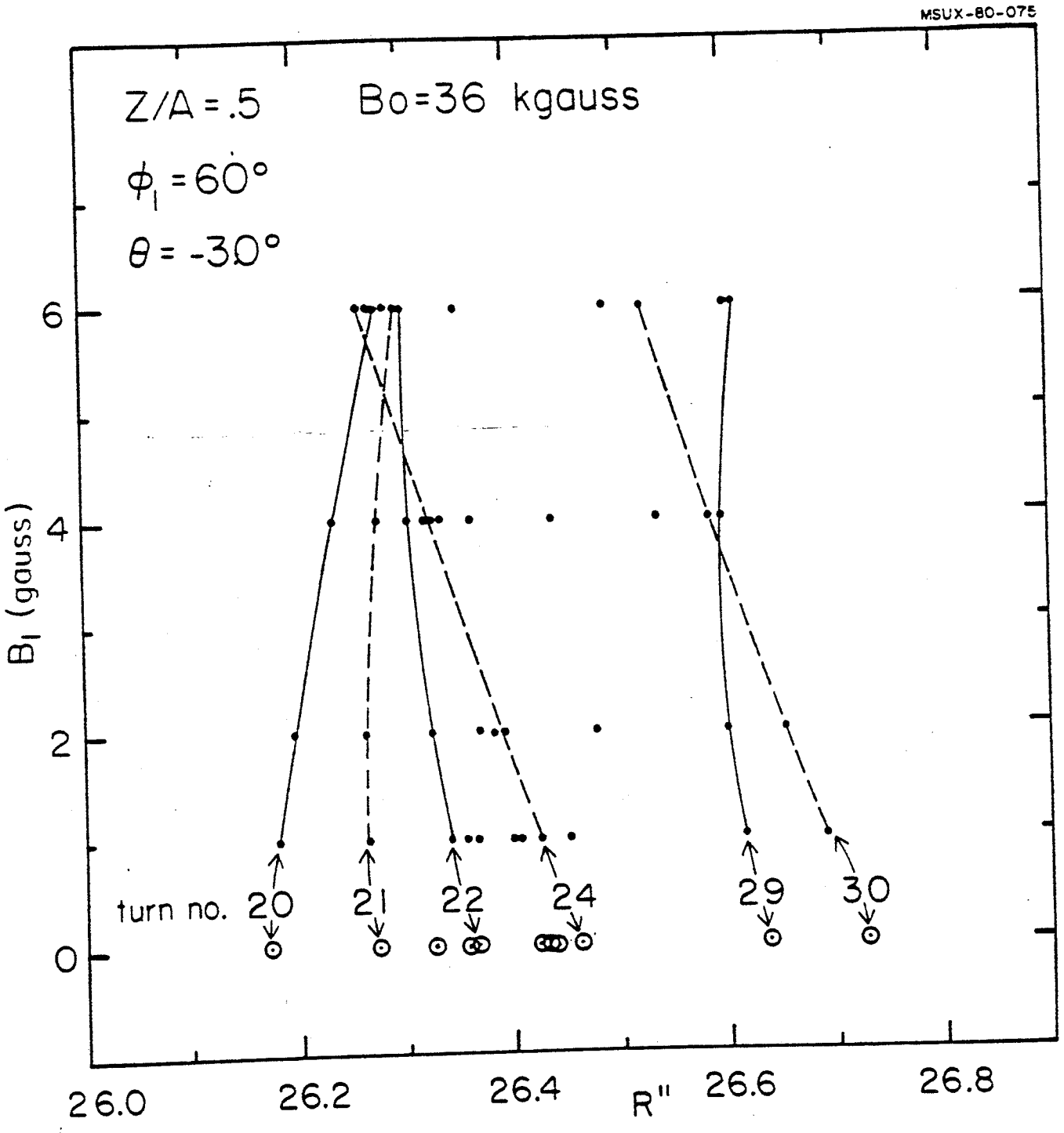

FIG. 11. Central ray radii near deflector entry for a variable 1st harmonic amplitude and a fixed phase $\phi_1=60^o$.

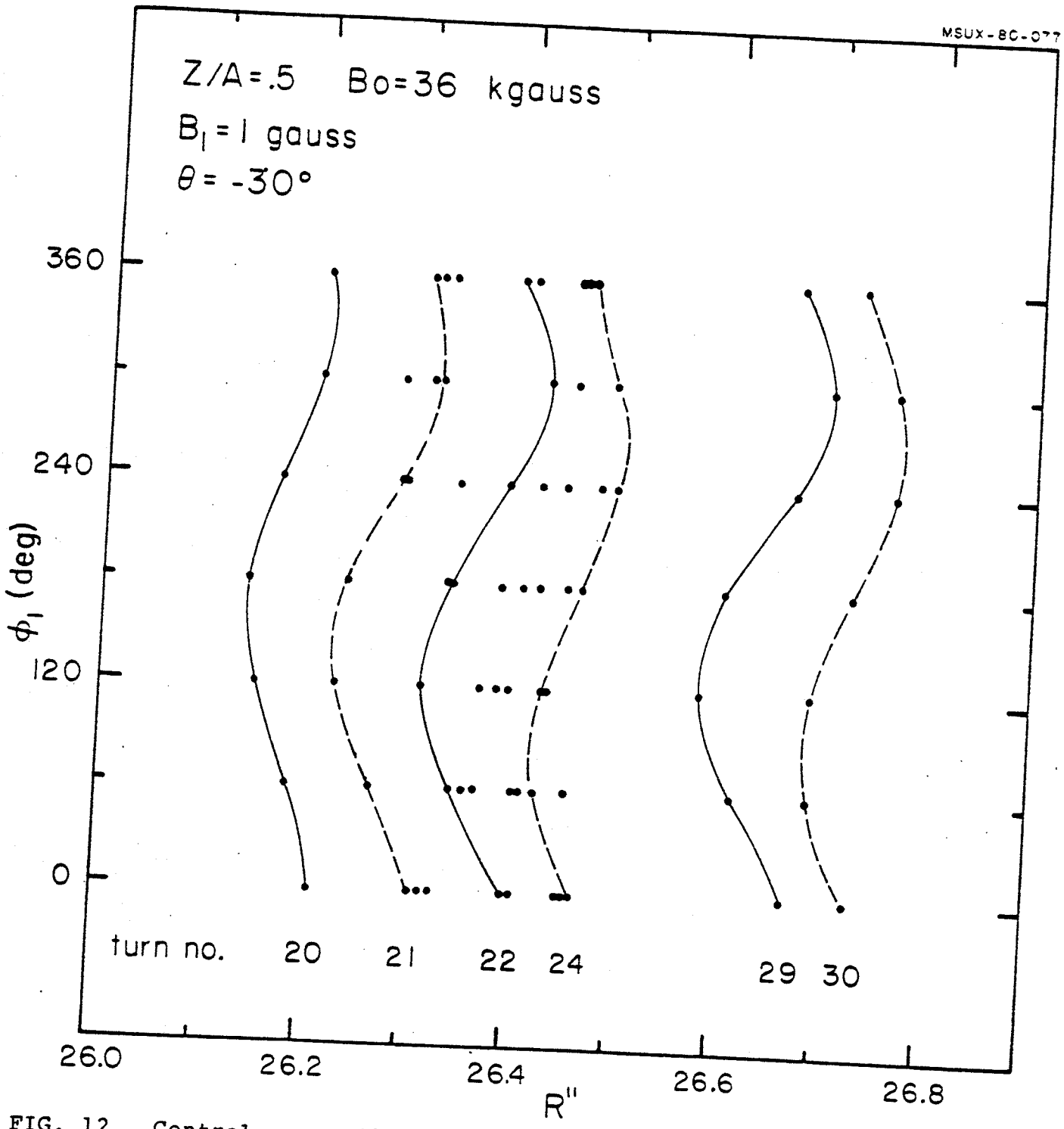

FIG. 12. Central ray radii near deflector entry for a variable 1st harmonic phase and a fixed amplitude B_1=1 Gauss.

themselves. For this case, a 1^{st} harmonic with B_1=1 gauss and $\phi_1=60^o$ is appropriate for a good turn to turn separation around the required radius of 26.5". Similar analyses yielded the proper 1^{st} harmonics parameters for all other ions.

The phase plots presented in the following were obtained by accelerating beams of 6-7 mm mrad emittance, both in the radial and axial phase space. The starting energy for each was selected several turns (typically 20 to 30) before the ν_R=1 resonance and the starting phase with respect to the R.F. is as given by equilibrium orbit data. Eight particles were chosen for representing each phase space, the initial conditions being determined by the eigenellipse at the starting azimuth and energy. Centering of the beam was also determined by trial and error, i.e. by accelerating the central ray, prior to the ν_R=1 resonance, and checking its behavior with respect to the equilibrium orbit.

The results for the radial phase space are shown in Figs. 13 through 20 and the main paramters pertaining to these calculations are also listed in Table II. The entries in this table are:

- Z/A, B_o : ion's charge to mass ratio and center field value
- T/A_I, T/A_F : starting energy for the acceleration and final energy at the angle $\theta=-30^o$ discussed above
- R_F, ϕ_F, ΔR : radius, phase with respect to RF and beam to beam separation at $\theta=-30^o$
- B_1, ϕ_1 : 1^{st} harmonic amplitude and phase used.

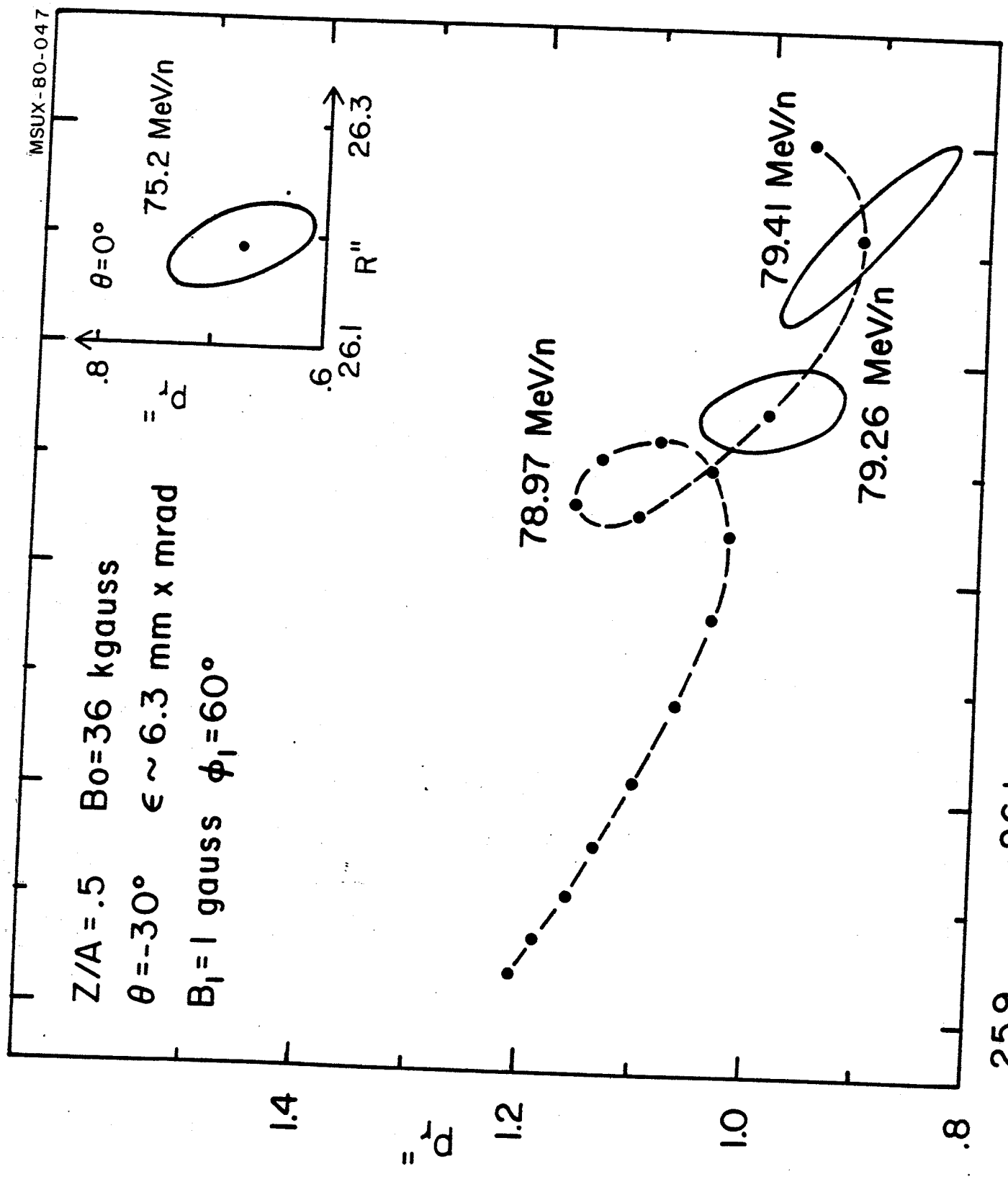

FIG. 13. Radial phase plot at extraction for the ion with Z/A = .5 and B_o=36 kgauss.

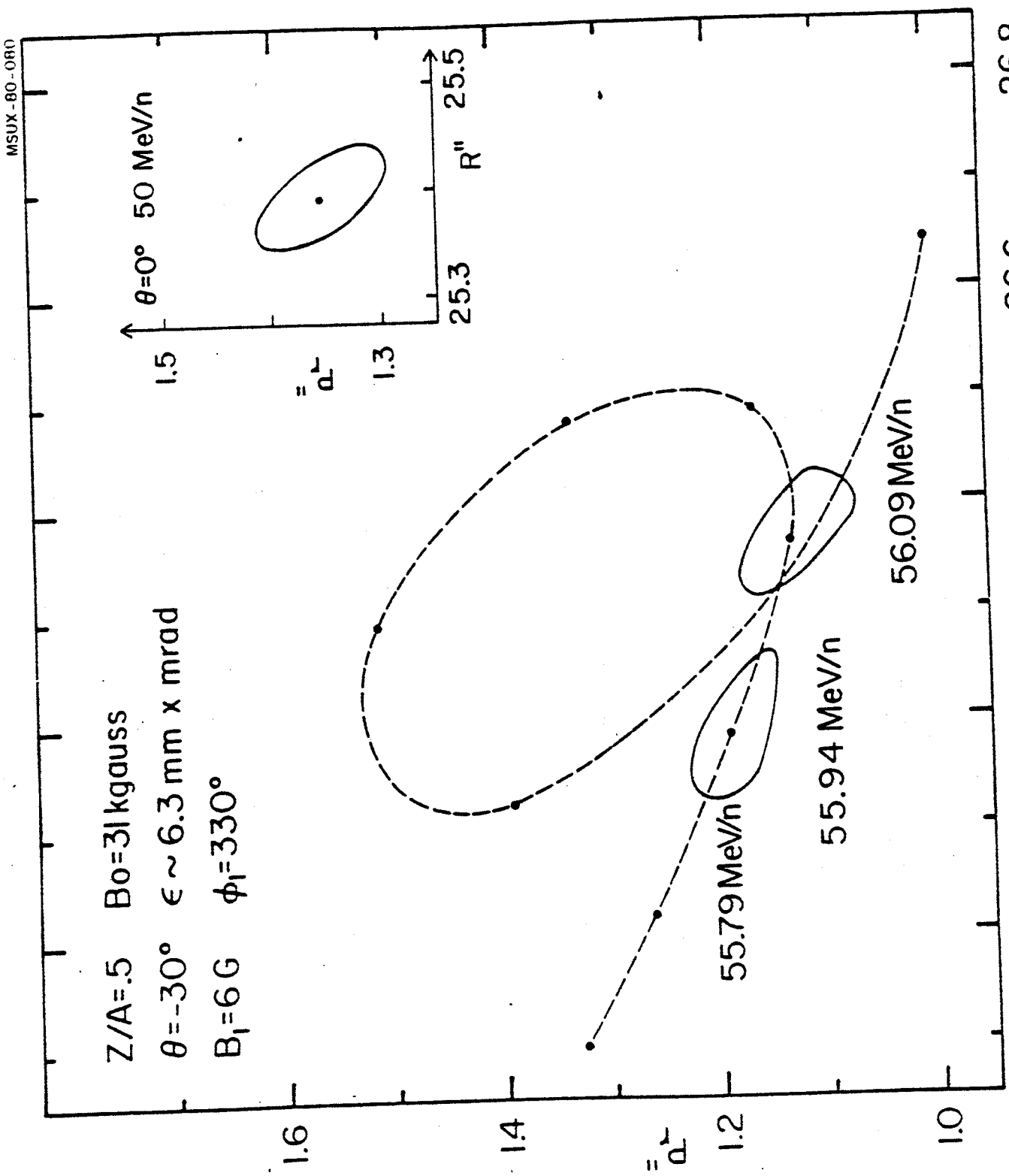

FIG. 14. Radial phase plot at the extraction for the ion with Z/A=.5 and B_o=31. kgauss.

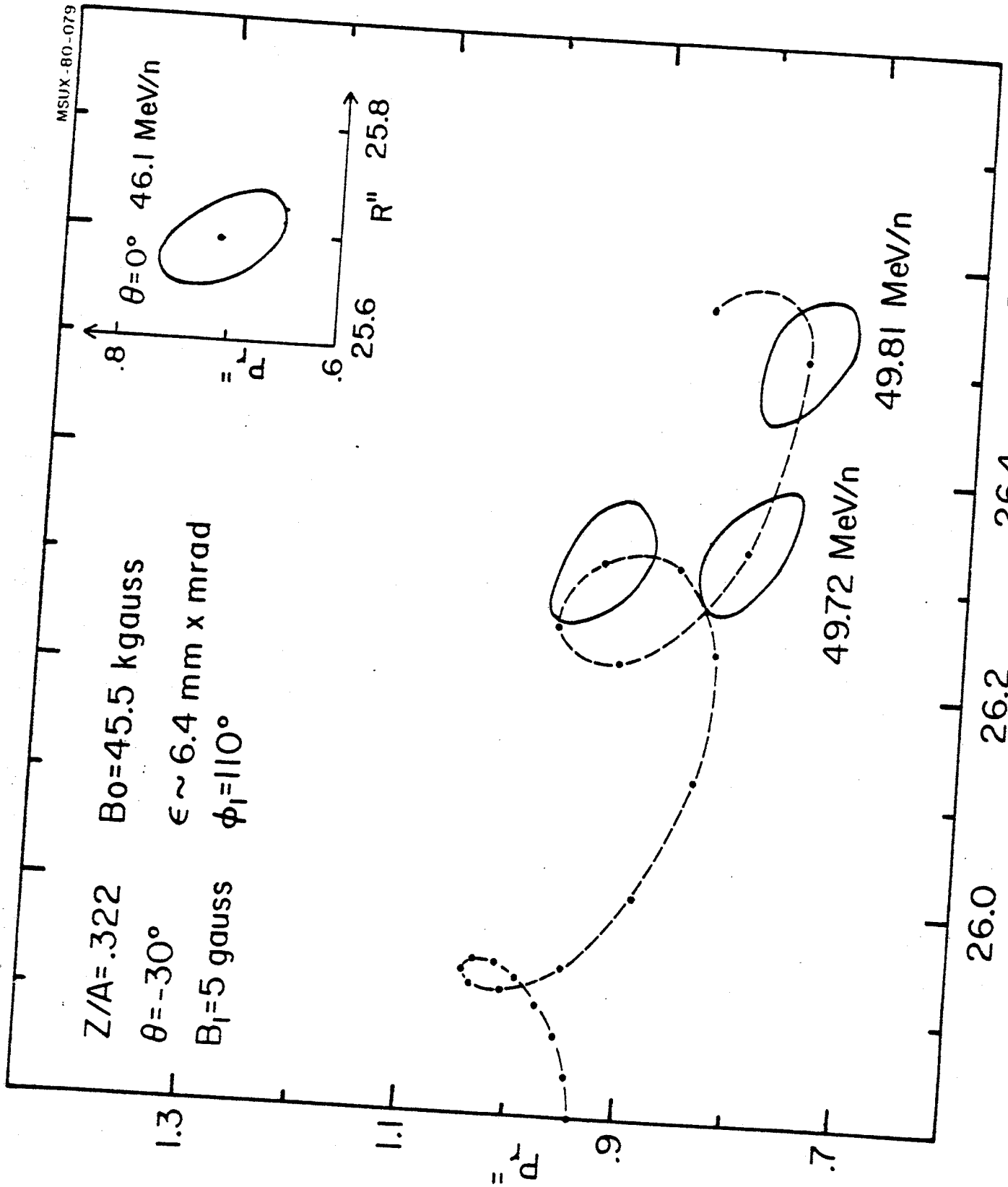

FIG. 15. Radial phase plot at the extraction for the ion with Z/A = .322 and B_o = 45.5 kgauss.

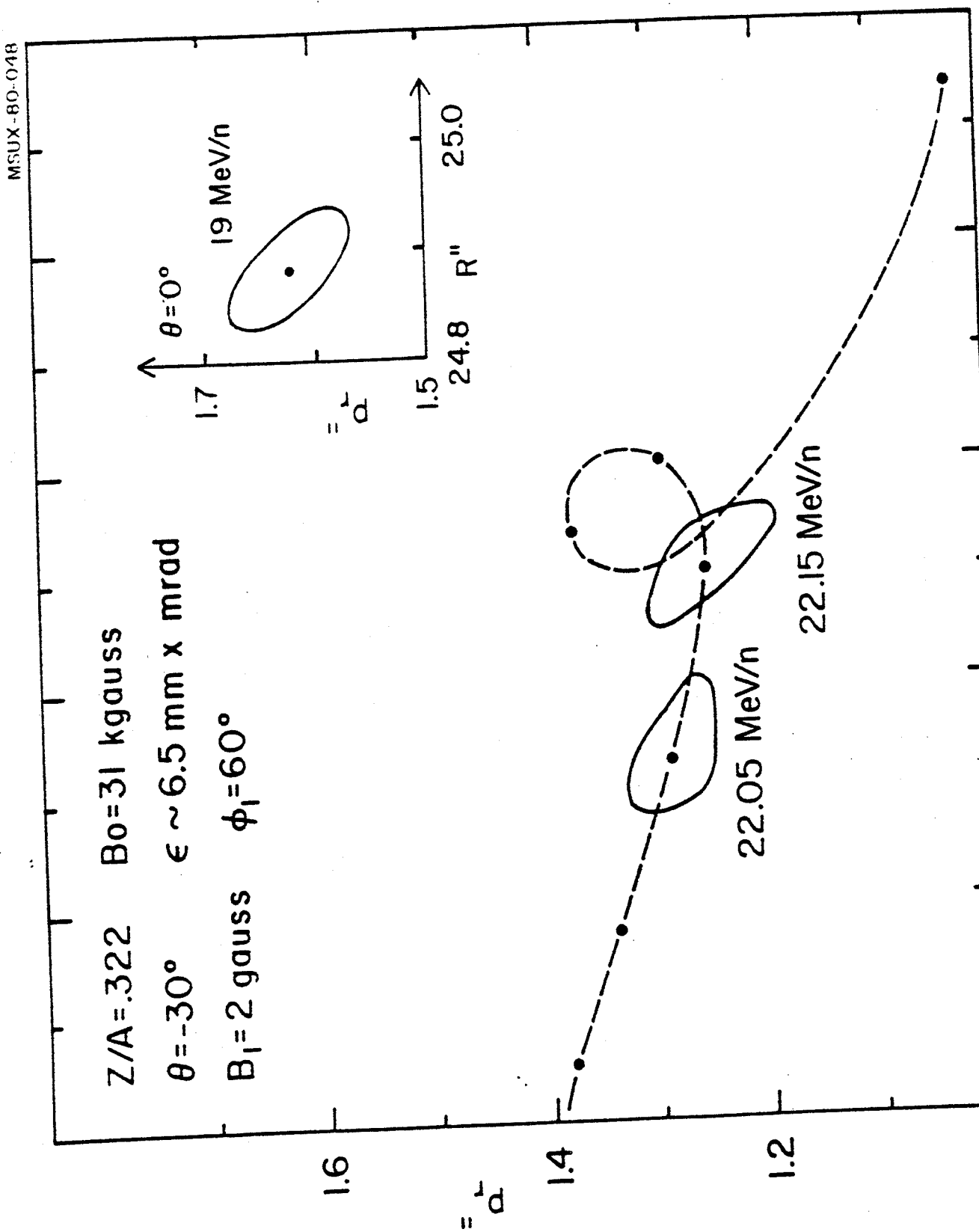

FIG. 16. Radial phase plot at the extraction for the ion with Z/A = .322 and B_o = 31. kgauss.

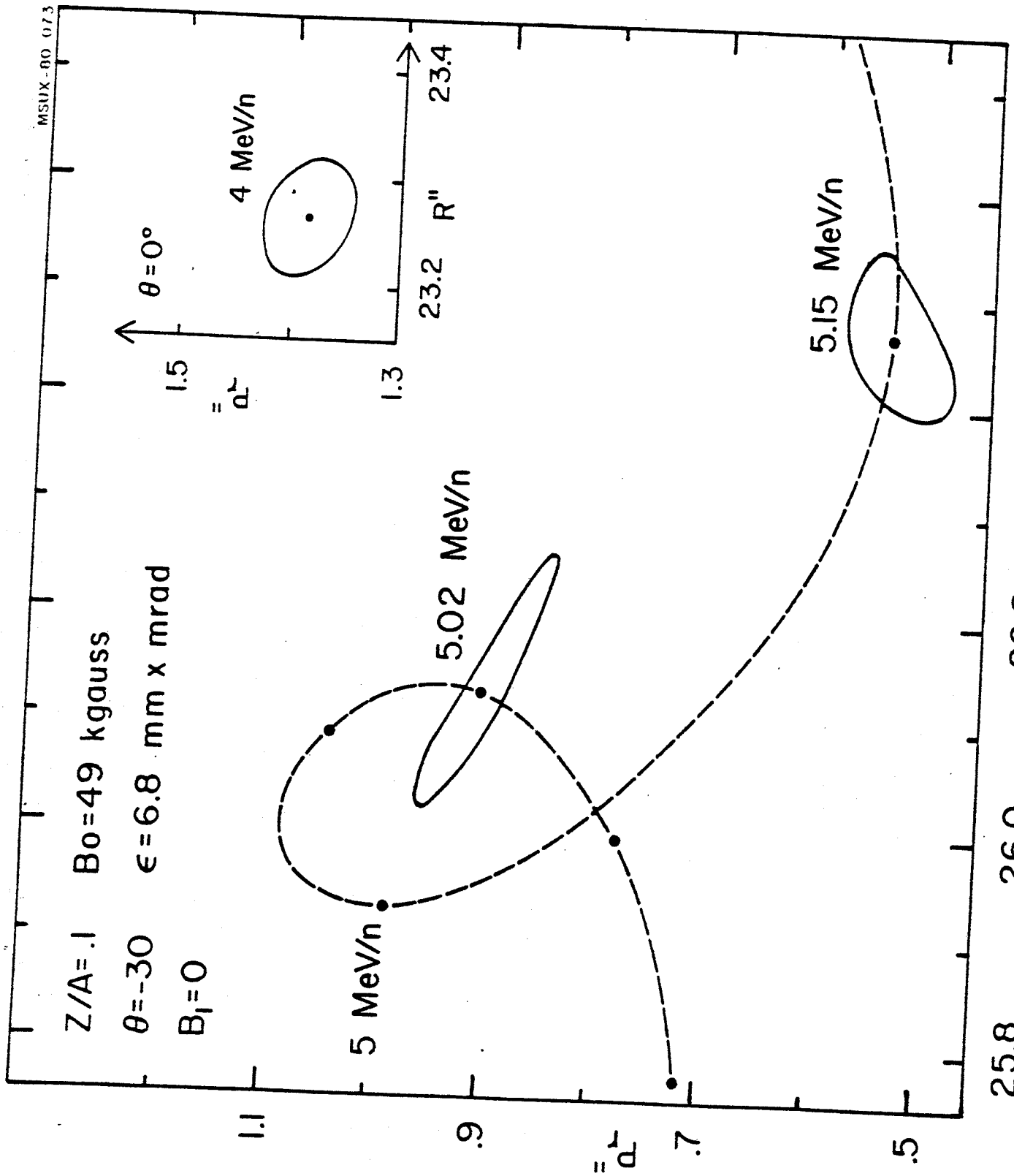

FIG. 17. Radial phase plot at the extraction for the ion with Z/A = .1 and B_o = 49. kgauss.

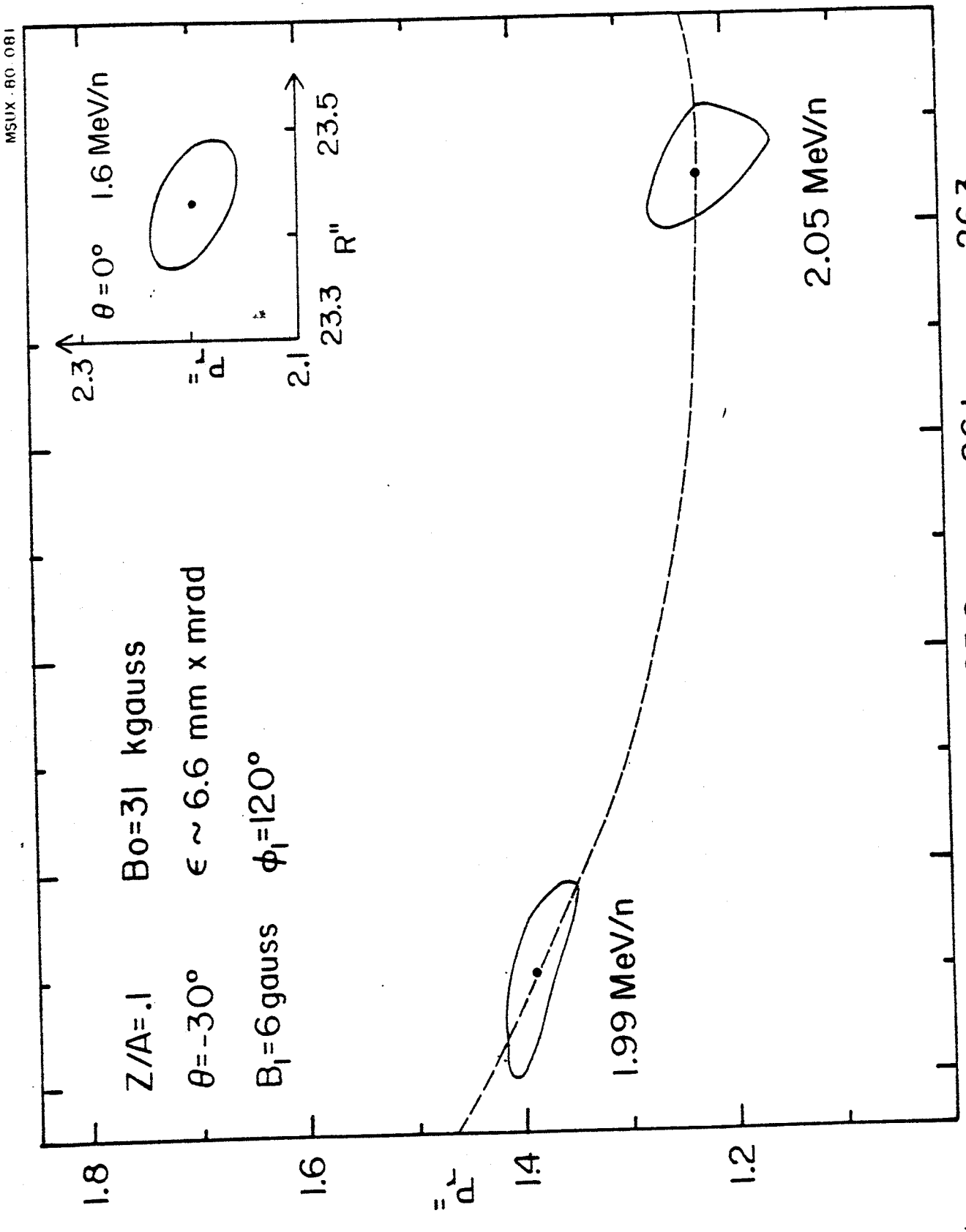

FIG. 18. Radial phase plot at the extraction for the ion with Z/A = .1 and B_o=31. kgauss.

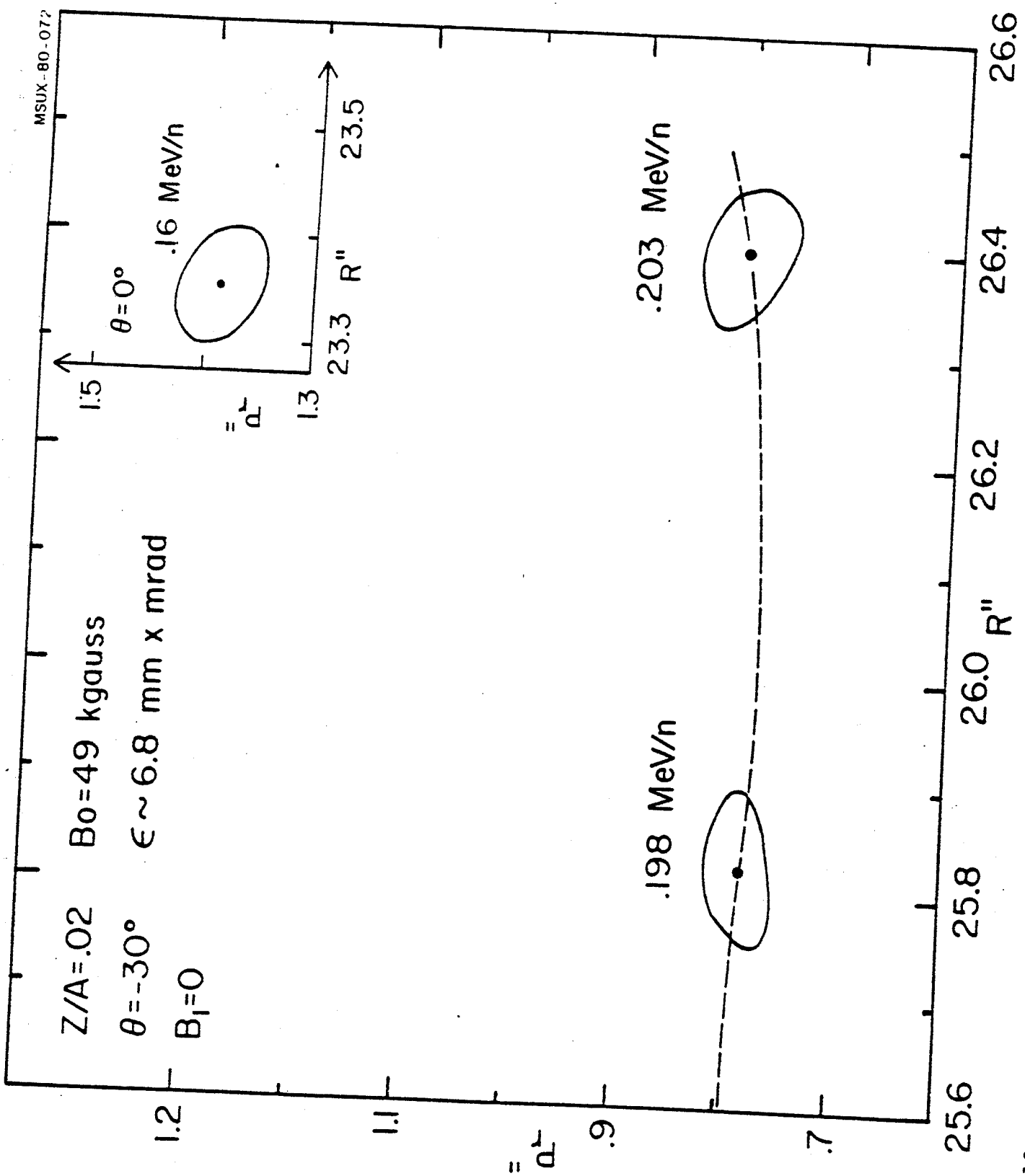

FIG. 19. Radial phase plot at the extraction for the ion with Z/A = .02 and B_o=49. kgauss.

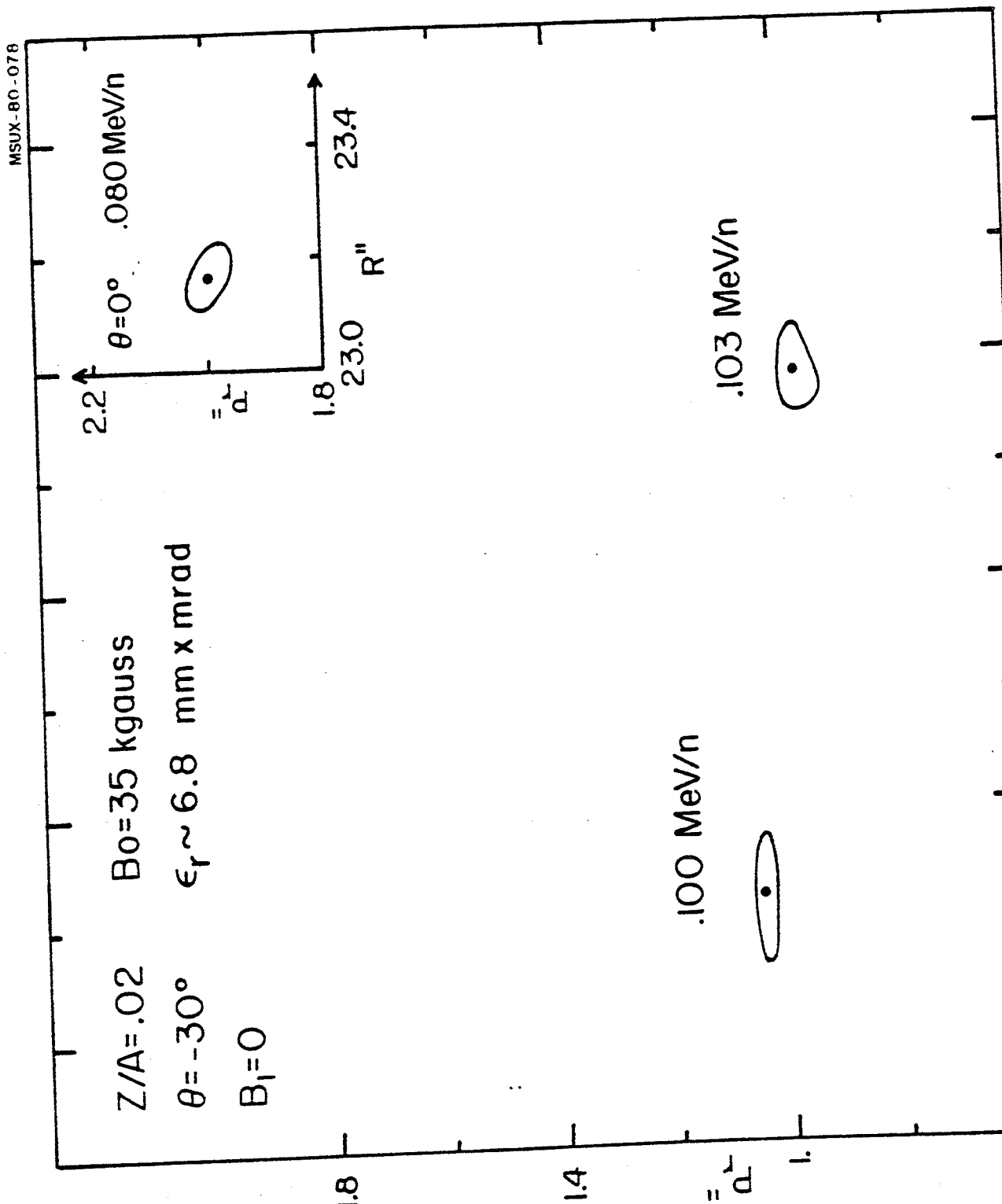

FIG. 20. Radial phase plot at the extraction for the ion with Z/A = .02 and B_o=35. kgauss.

Table II. Acceleration data for representative ions

Z/A	B_o (kG)	T/A_I (MeV/n)	T/A_F (MeV/n)	R" (θ=-30°)	ϕ_F (deg)	ΔR (mm)	B_1 (G)	ϕ_1 (deg)
.5	36.6	75.2	79.41	26.61	17.	1.	1.	60.
.5	31.	50.	56.09	26.36	8.	1.3	6.	330.
.32	45.5	46.1	49.81	26.51	19.	1.5	5.	110.
.322	31.	19.	22.15	26.30	6.	1.	2.	60.
.1	49.	4.	5.15	26.47	31.	3.4	-	-
.1	31.	1.6	2.05	26.35	16.	15.5	6.	120.
.02	49.	.16	.203	26.40	21.	10.9	-	-
.02	35.	.08	.103	26.37	23.	19.05	-	-

For all the figures 13-20 only the last two phase plots, i.e. the one relevant to the turn prior to extraction and the "extracted" one are presented, while central ray positions are given for all turns allowed by the radial scale range. Also shown is the initial phase space, determined as explained above. Since every figure lists in a self explanatory way all relevant parameters, we shall just discuss here the general trend which emerges.

- Adequate beam to beam separation can be achieved in all cases. The letter is of the order of 1 mm, or slightly more for high energy beams, i.e. stand-alone cases with a large turn number (Z/A=.5 or Z/A=.322). The separation increases enormously, as it is obvious, for the injector-mode beams, where it attains several mm. In fact, as apparent from Table I, the peak dee voltage has been lowered in these cases below the nominal 100 kV value.

- The central-ray radial positions at $\theta=-30^{o}$ vary from 26.3" to 26.6". The situation is summarized in the (r,p_r) plane and for all eight ions, in Fig. 21. The lowest radii belong to the low B_o values, as can also be seen in Figs. 14, 16, 18, and 20. This however, does not stem from any difficulty in achieving a proper turn to turn separation at larger radii but rather from the rapid approaching of the $\nu_R + 2\nu_Z=3$ resonance. In fact the axial phase space tends to deteriorate rapidly at these radii as will be seen presently. Attempts to further restrict such a radial range of deflector positions have failed just because of this.
- Distortions seem to be very limited in all cases, and in fact in most instances they are negligible. However, this will be discussed in more detail in the next paragraph.
- The 1^{st} harmonic amplitude is confined within very reasonable limits, as a glance to Table II will show.

The axial phase space behaviour is shown in Figs. 22 and 23, for the four stand-alone beams and the four injector-mode beams respectively. Both the starting and "extracted" phase spaces are plotted. It will be noted that only in the case of low fields the axial phase space does exhibit some blow-up, which, at $\theta=-30^{o}$, is demonstrated by the increase in p_Z values. The effect is quite evident for the .5/31 and .1/31 ions, and less for the .322/31 case which, as shown in Fig. 21, belongs however to the most internal radius.

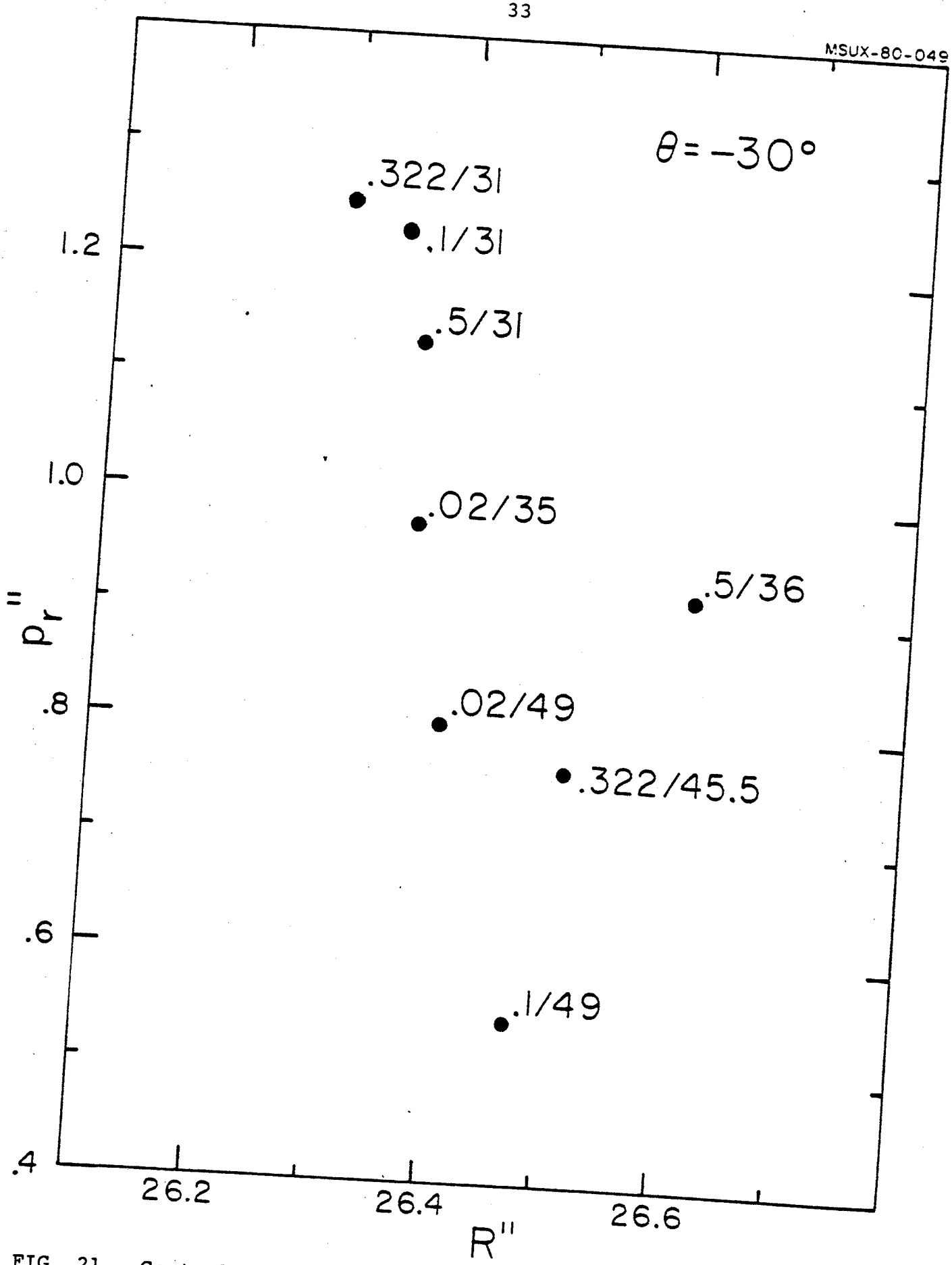

FIG. 21. Central ray coordinates in the (p_r,R) space at $\theta = -30^\circ$ for the eight ions listed.

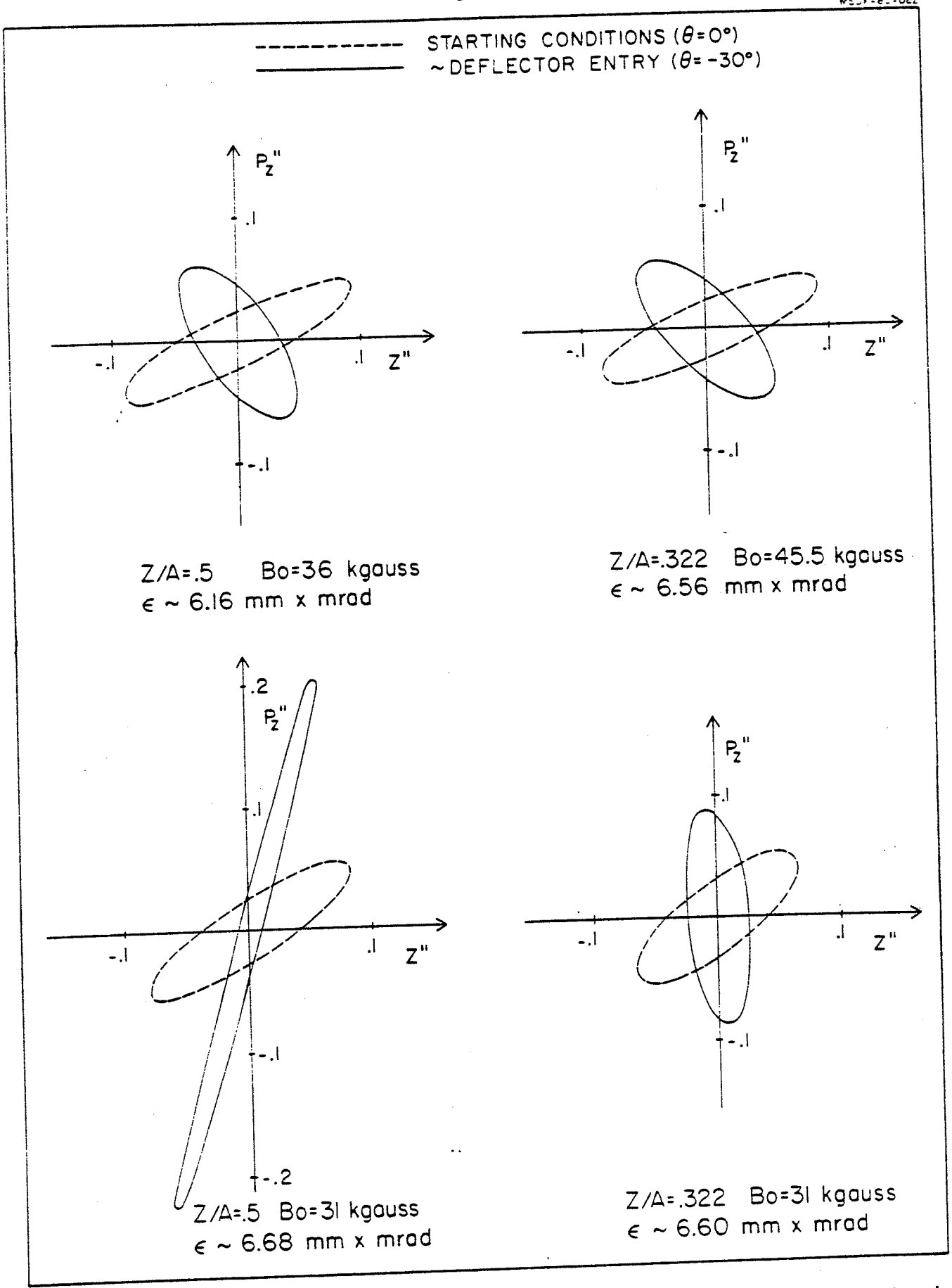

FIG. 22. Axial phase space for four "stand alone" beams at the beginning of acceleration and at deflector entry.

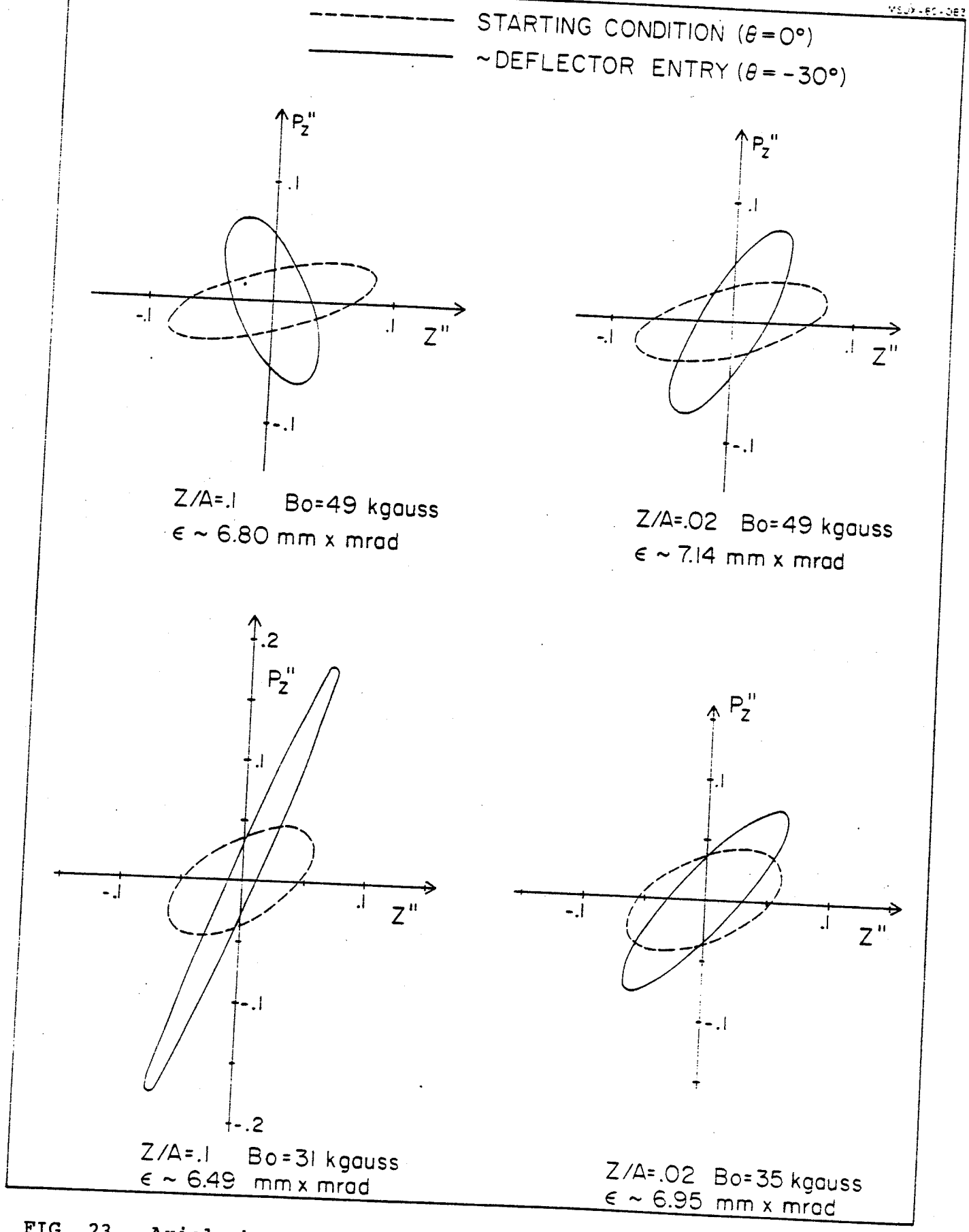

FIG. 23. Axial phase space for four "injector" beams at the beginning of acceleration and at deflector entry.

Should one try to extract a few turns later, the axial phase space could no longer be confined. The choice of a radially movable deflector is therefore fully justified, in our case, because on one side it minimizes electric fields requirements on the deflectors by allowing to extract at the farthest out radii for very relativistic particles. On the other hand, when the presence of the resonances requires to extract at more internal radii, a movable deflector allows just this and therefore the beam quality in the axial phase space is preserved. It should also be noted that in the latter case the electric fields needed are usually less critical.(5)

4. Radial Phase Space Distortions

Radial phase space distortions in proximity or in the crossing of resonances like the $\nu_R=1$ are a well known fact in AVF cyclotrons. Excessive field bumps are their principal cause and under these conditions they are observed in a superconducting cyclotron as well. These distortions do not warrant therefore further consideration.

In this section, however, we want to present in some detail evidence for distortions which are observed even in absence of any imperfection in the magnetic field and seem in fact generated by the rather tight spiral of the dees. In this sense therefore they are relatively unexpected and in a way peculiar to the typical design of a superconducting cyclotron.

For the K-500 cyclotron we have carried out the bulk of this analysis on the ion with Z/A = .1 and B_o=31 kgauss,

i.e. a final energy of ~2. MeV/n which is reached in only 40 turns. The low turn number and therefore the fast crossing of the $\nu_R=1$ resonance would lead to expect minimal distortions. In fact this is not the case, as shown in Fig. 24, where at $\theta=-30^o$ a severe distortion is observed. The case shown here refers to a "realistic" acceleration, namely the field includes the perturbations due to the magnetic channels and their compensation, and to a first harmonic of $B_1=6$ gauss with a phase $\phi_1=80^o$.

However, it was quickly realized that this distortion does not depend in a sensible way, from either the accelerating conditions (i.e. starting energy, dee voltage) or the presence of the first harmonic of 6 gauss. This is shown in Fig. 25 where no first harmonic is used, and two different dee voltages are employed. A further check with a field having a perfect 120^o symmetry, i.e. eliminating also the magnetic channels perturbations, yielded again the same distortions (Fig. 26). The latter quite unexpected result led therefore to a systematic study of all remaining causes of the distortions.

We carried out a further analysis of the possible influence of the accelerating phase and of the energy gain, using the 120^o symmetric field. A constant energy gain/turn, i.e. eliminating any phase dependence, has been used for obtaining the results of Fig. 27 where the dee voltage has been varied between 26 kV and 125 kV. The distortions, although with some alterations, are always present. They tend to be smaller, though, when the dee voltage is lowered to 26 kV, thus increasing considerably the turn number. We then turned to an analysis of the effects

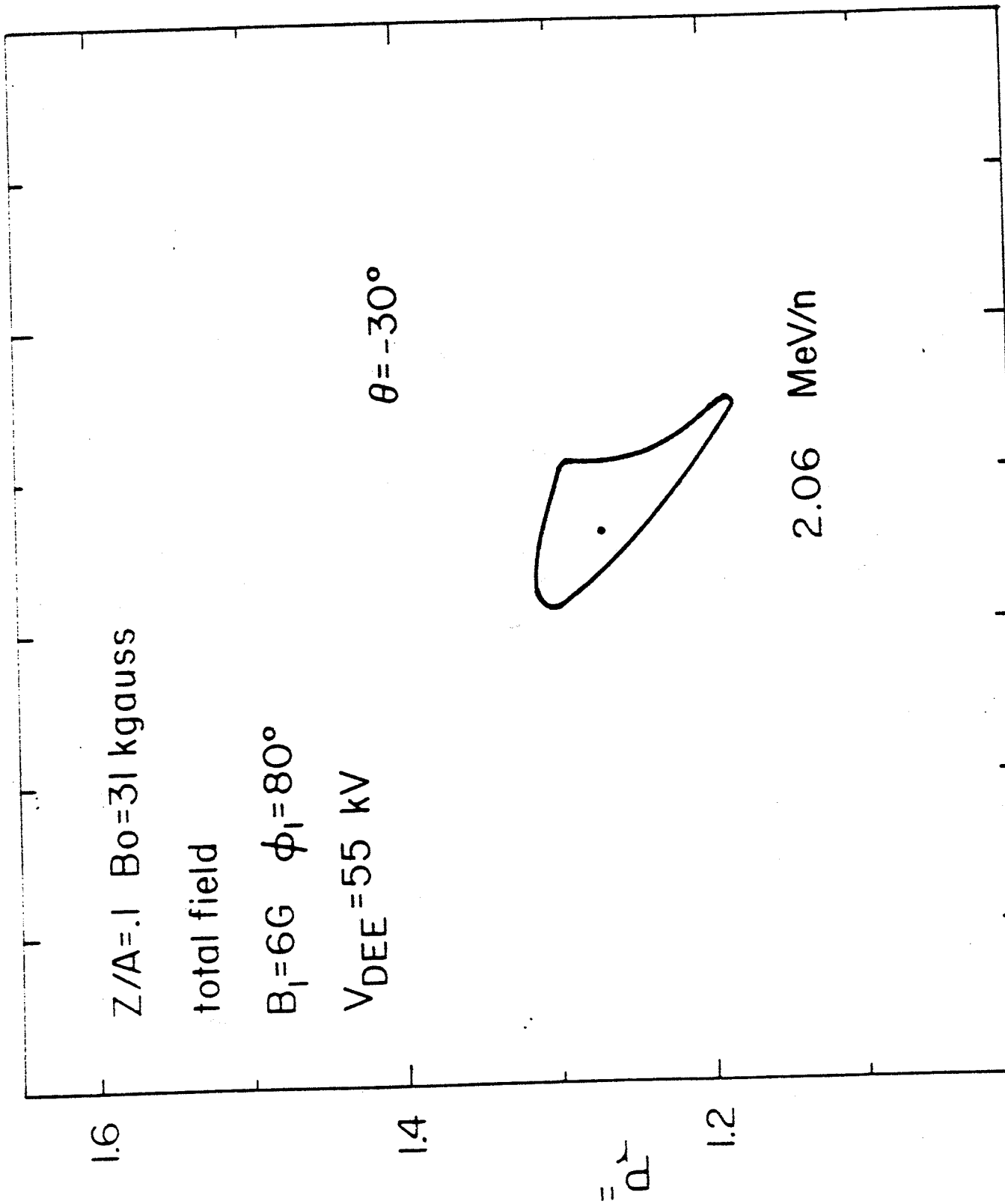

FIG. 24. Radial phase space at the extraction for an ion with Z/A = .1 and B_o=31. kgauss (see text for details).

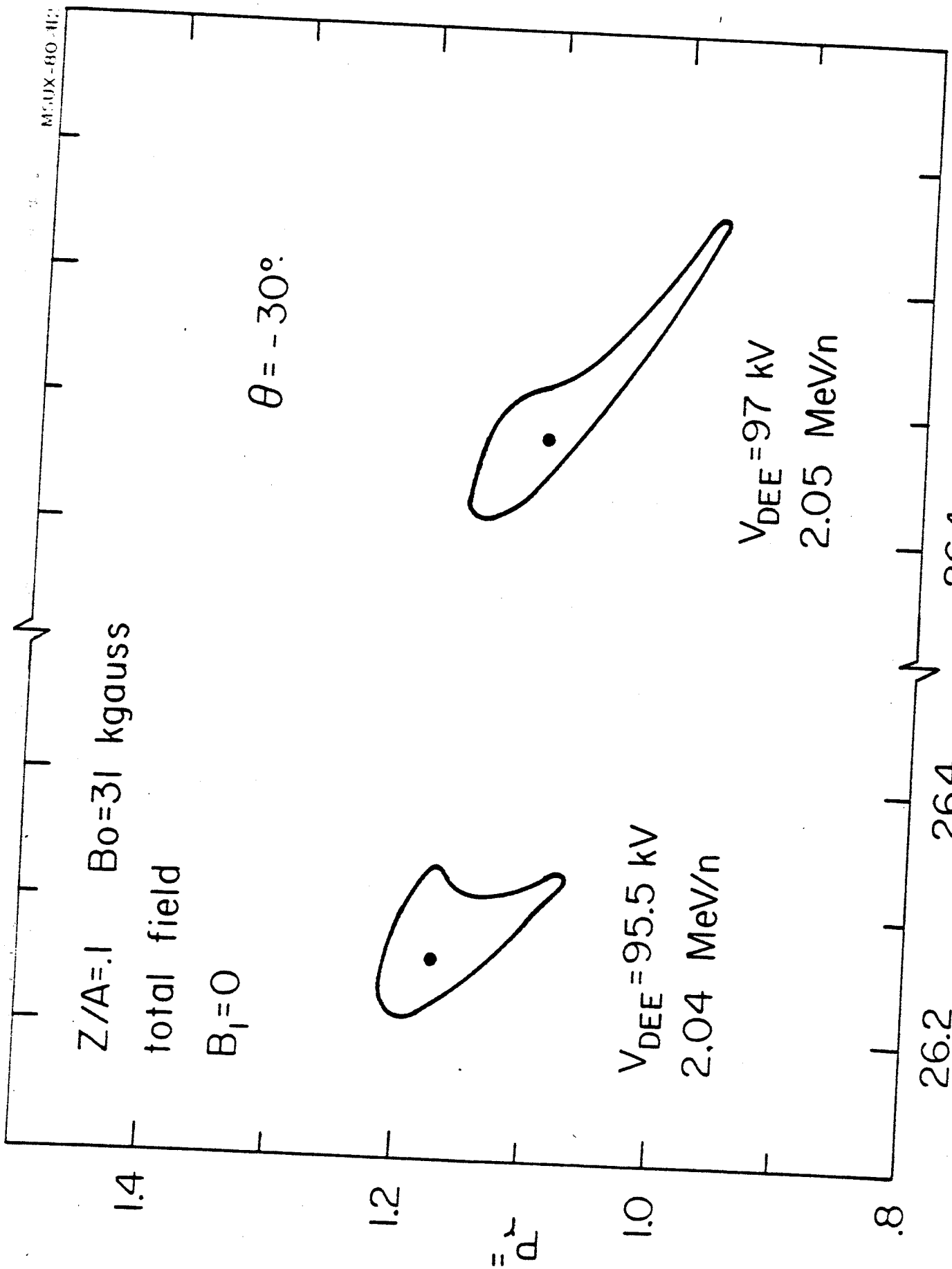

FIG. 25. Radial phase space at the extraction for the same ion of Fig. 24 and with different dee voltages.

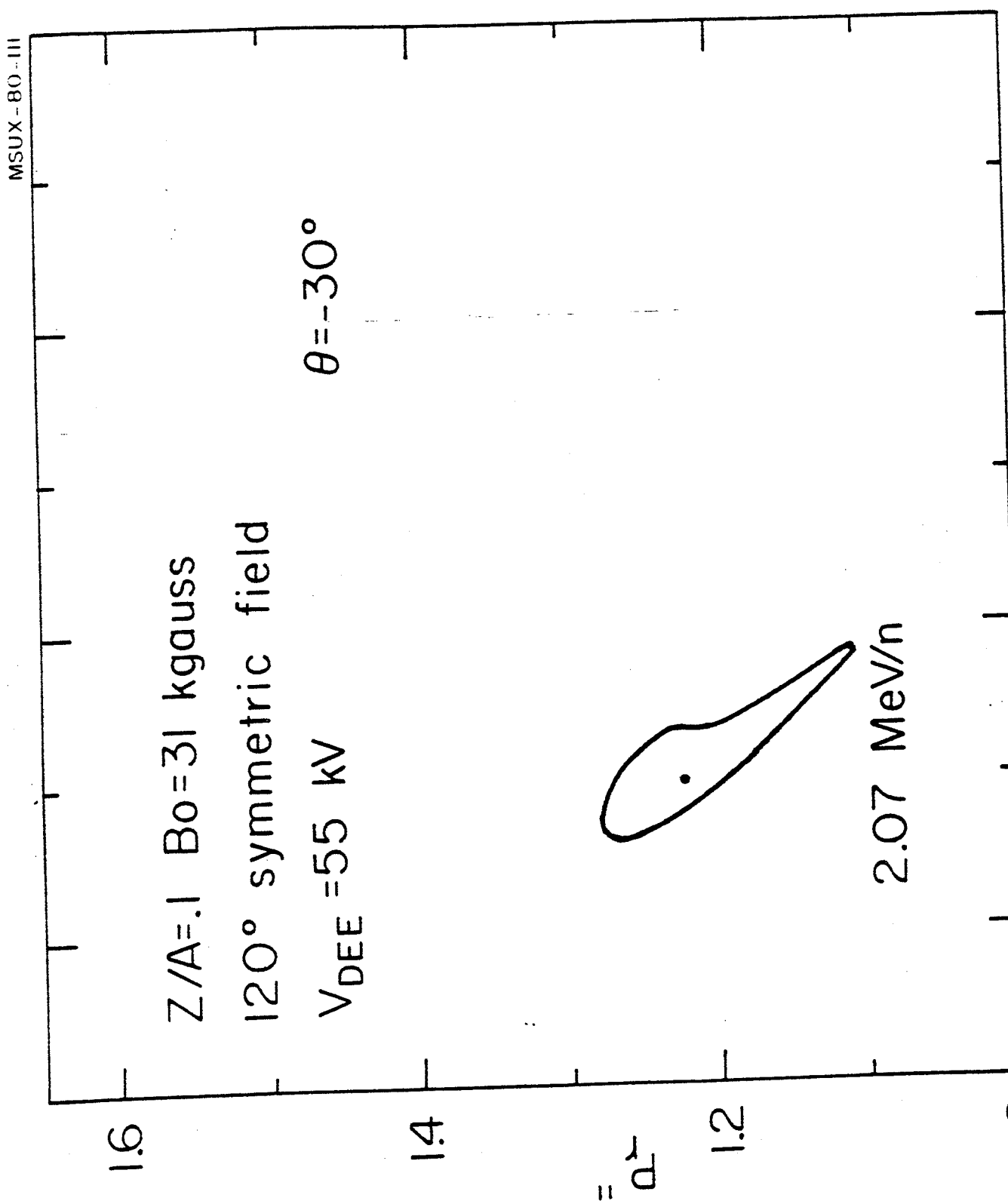

FIG. 26. Radial phase space at the extraction for the same ion of Fig. 24 accelerated in the 120° symmetric field.

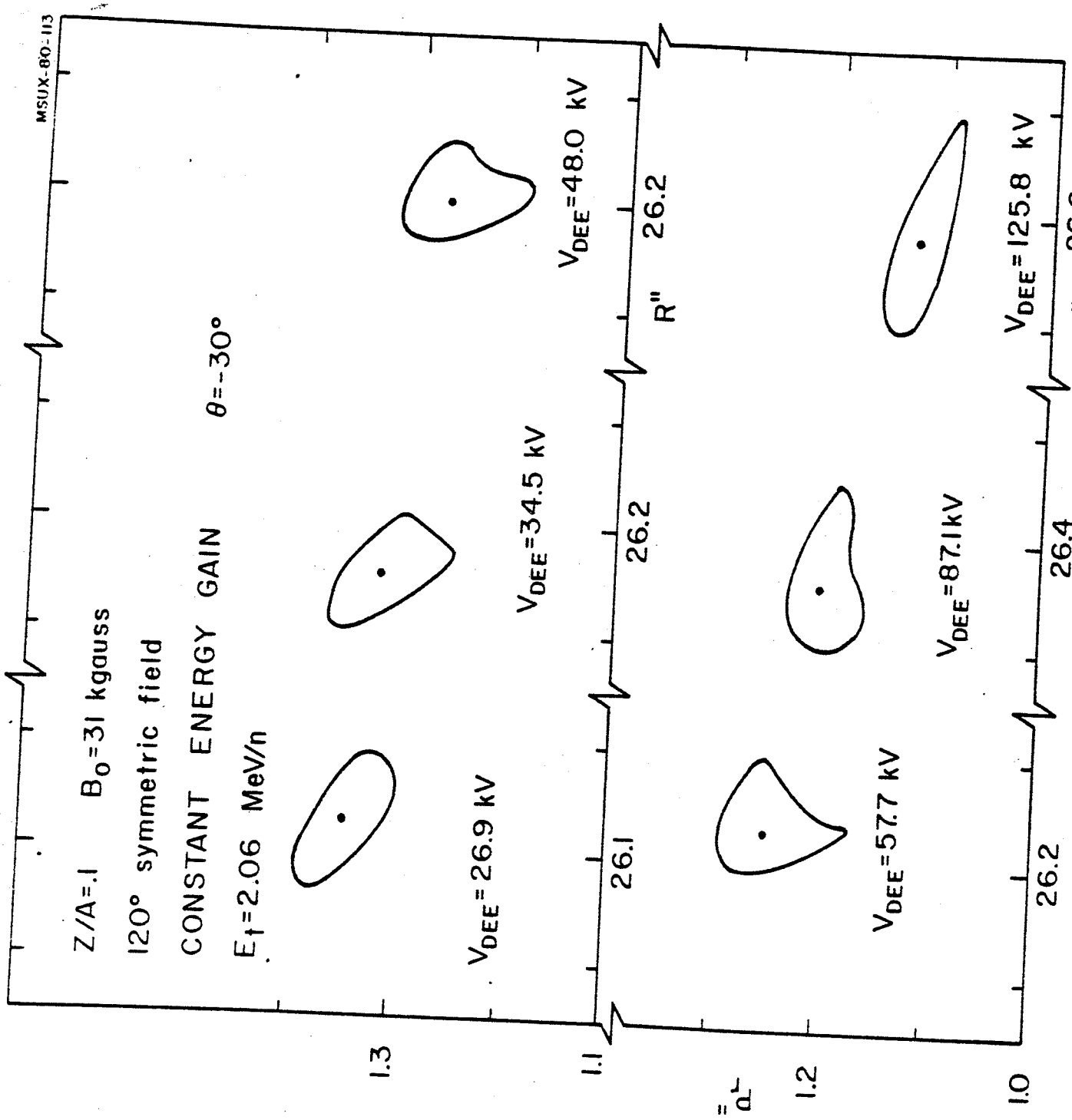

FIG. 27. Radial phase space at the extraction for the same ion of Fig. 25 accelerated with a constant energy gain/turn and different dee voltages.

of the dee spiral. Spiral constants of 0., -2.204, -4.407 and -6.611 deg/inch were tested. Let us recall that -4.407 deg/inch corresponds to the actual spiral constant of the machine, and 0. obviously assumes radial dees. The results, again for a 120^{o}-symmetric magnetic field are shown in Fig. 28, the energy gain/turn being constant with a dee voltage set to 57 kV. The figure shows unmistakable evidence of the dee spiral effect, i.e. the accelerated ellipse is progressively more distorted the larger the spiral constant, while for radial dees it remains practically undisturbed by the resonance crossing. This is the case also for all dee-voltages previously investigated in Fig. 27. Moreover, if radial dees are assumed and the beam accelerated under the same conditions as of Figs. 24 and 25, i.e. realistic magnetic fields including purturbations, then one obtains the phase plots shown in Figs. 29 and 30 respectively. The comparison between the two sets of otherwise identical cases clearly points out the importance of the dee spiral.

These findings obviously do not imply that all distortions can be traced back to the dee spiral effect. As stated above those distortions generated by the first harmonic and overall field imperfections will be present regardless of the dee-spiral. It looks therefore like the dee-spiral effect is particularly sensitive for ions with a low turn number and thus a remarkable non-adiabatic acceleration process. This is supported by the results just discussed and the fact, previously mentioned, that also for the actual spiral the distortions tend to be minimized the lower the dee-voltage

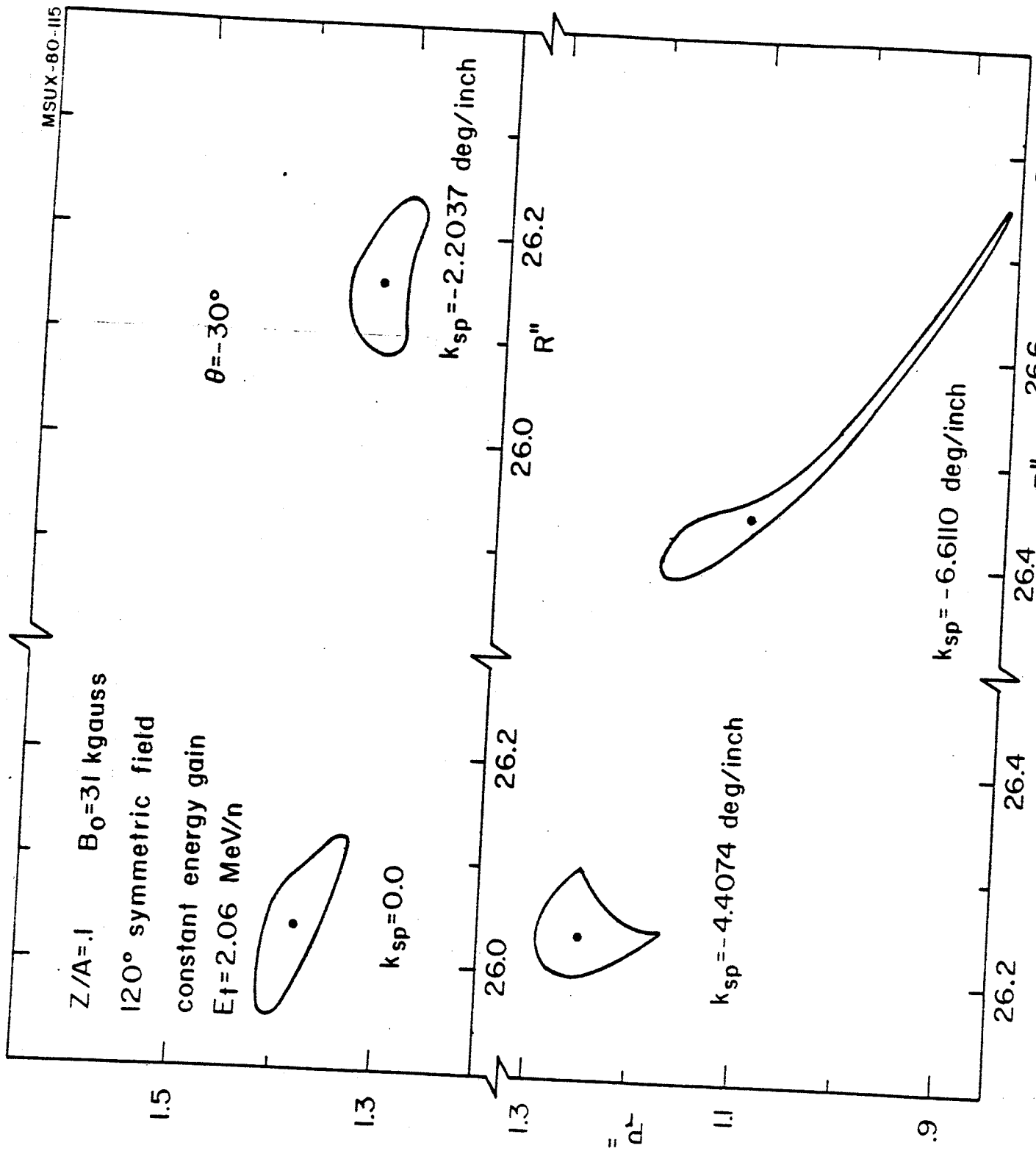

FIG. 28. Radial phase space at the extraction for the same ion as Fig. 24 accelerated with dees having different spiral constants and dee voltages equal to 57. kV.

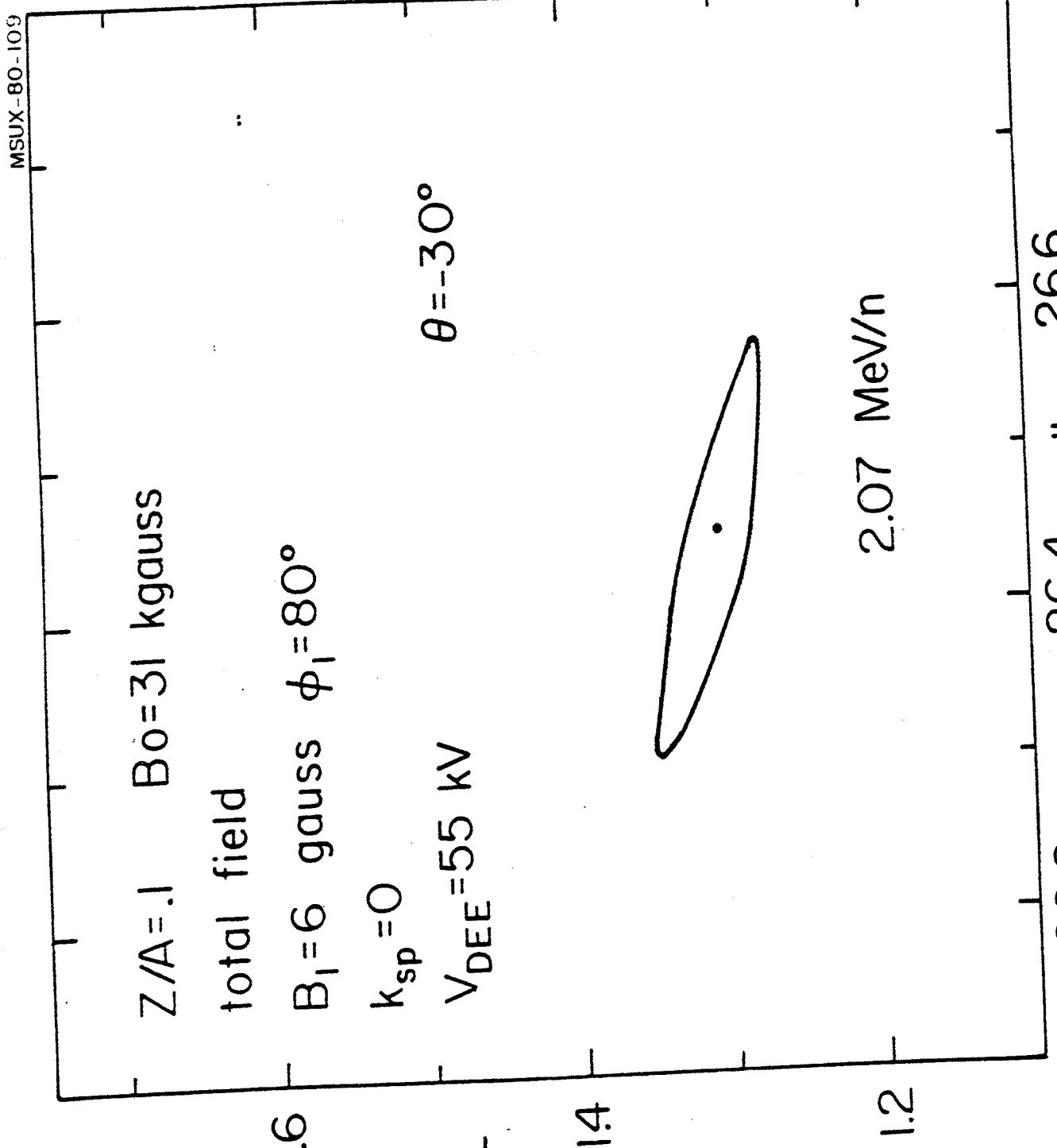

FIG. 29. Radial phase space at the extraction for an ion with Z/A = .1 and B_o=31. kgauss accelerated under the same conditions of Fig. 24, but with radial dees.

(Fig. 27). A likely explanation is that for low turn-number beams the intrinsic off-centering generated by the acceleration process gives rise, in turn, to sizable differences in the radial momentum acquired at each dee gap traversal, if the dees have a tight spiral shape. This process can excite the resonance much the same way a field first harmonic does. In fact the distortions generated by a spiraling dee in an otherwise perfectly 120^{o} symmetric field can be reproduced with a radial dee, in the same field to which a suitable first harmonic is added.

As a consequence a first harmonic of suitable amplitude and phase can be used to compensate for the spiral-dee effect for those low turn number beams where the spiral effect is dominant. Precisely this has been done in the case of the .1/31 ion, as previously shown in Fig. 18, where a first harmonic of B_1=6 gauss and $\phi_1=120^{o}$ was employed.

It is indeed interesting that for these low turn-number beams, where turn to turn separation at the deflector entrance is never really an issue, the first harmonic can be used to compensate for acceleration induced distortions.

5. Conclusions

This survey of beam dynamics for the K-500 cyclotron shows that no difficulties should be encountered in obtaining proper beams for subsequent extraction. While many of the beam dynamics features are quite analogous to those of conventional AVF cyclotrons, a fundamental difference lies in the presence of the $\nu_R + 2\nu_Z=3$ resonance.

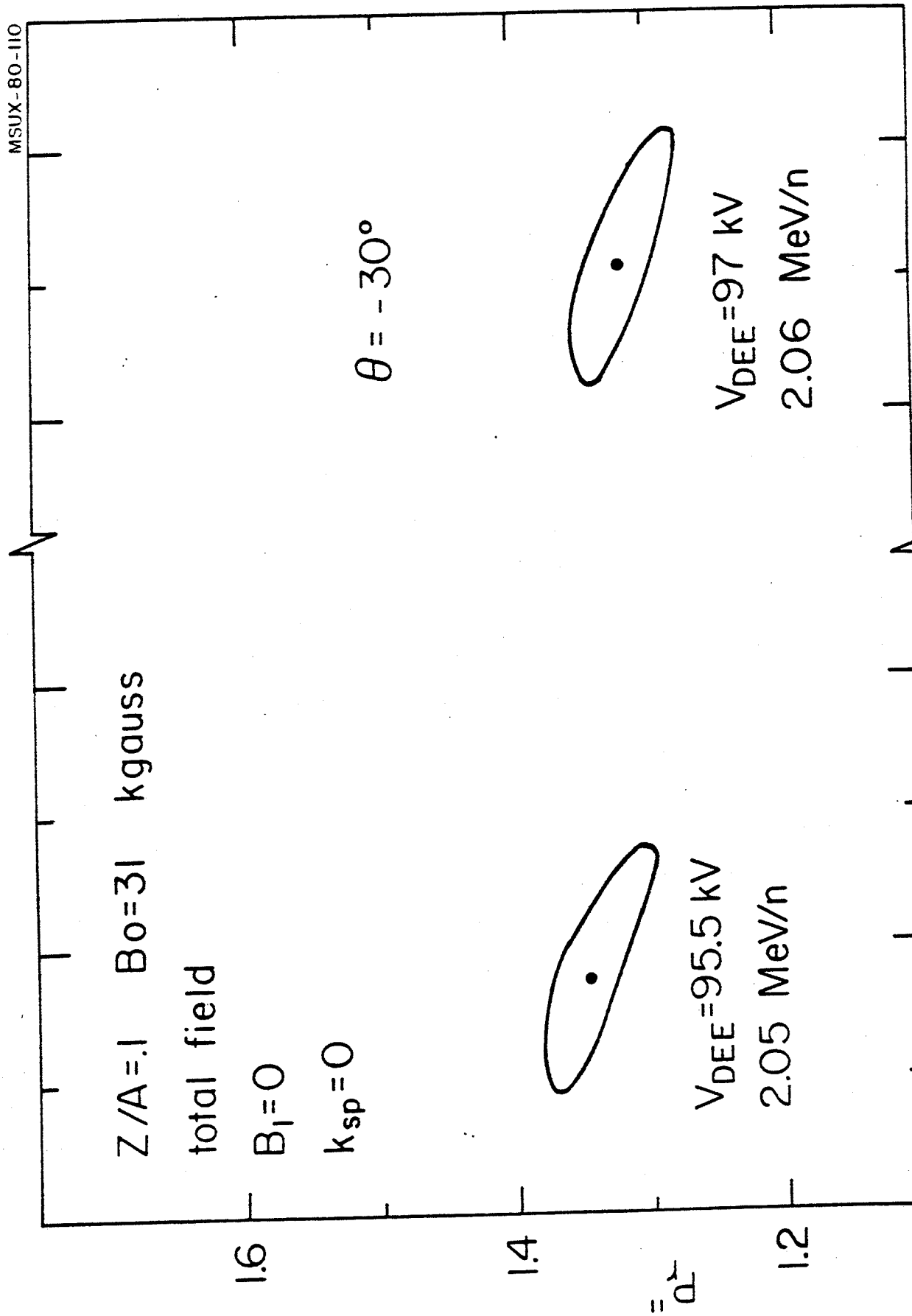

FIG. 30. Radial phase space at the extraction for ions with Z/A = .1 and B_o=31. kgauss accelerated under the same conditions of Fig. 25, but with radial dees.

While by no means jeopardizing the overall cyclotron performance, the resonance sets nevertheless limits to:

- the lowest operational field.
- the highest Z/A of ions which can be accelerated, i.e. the use of $^{3}He^{++}$ or protons is rather doubtful.
- At the same time the resonance also forces, more or less, to have radially movable extraction elements if a wide dynamic range of the machine is desired, as in the present case.

Finally one should remark the presence of distortions, for low turn-number beams, arising from the tight dee-spiral. They seem however to pose no large problem, since once the mechanism is known they can be essentially compensated for.

It is expected that since the fields used in this study are highly realistic, only minor numerical variations of the results presented here will be necessary when the same study will be carried out in the final magnetic field configuration.

REFERENCES

1. H.G. Blosser, D.A. Johnson; Field calculations for the MSU 500 MeV Superconducting Cyclotron Magnet. MSUCP-28 (1977), unpublished.
2. G. Bellomo, F. Resmini, Trimming of the Magnetic Field for the K-500 cyclotron at MSU, to be published.
3. D. Johnson; SPIRAL GAP CODE, private communication. - M.M. Gordon; Effects of Spiral Electric Gaps in Superconducting Cyclotrons, Nuclear Instruments and Methods 169 (1980) 327.
4. M.M. Gordon, E.M. Fabrici; Beam Extraction System for the K=500 Superconducting Cyclotron, IEEE Transitions on Nuclear Science, NS26 (1979) 2101.
5. E. Fabrici, D. Johnson, F.G. Resmini; The Extraction System for the K-500 Cyclotron at MSU, to be published.
6. G. Bellomo, D. Johnson, P. Miller, F. Resmini; Magnetic Field Mapping of the K-500 Cyclotron at MSU, to be published.
7. H.G. Blosser, et al., MSUCL-222A (1976), unpublished - H.G. Blosser; The Michigan State University Superconducting Cyclotron Program, IEEE Transections on Nuclear Science, NS26 (1979) 2040.
8. F. Resmini, G. Bellomo, E. Fabrici, H.G. Blosser, D. Johnson; Design Characteristics of the K=800 Superconducting Cyclotron at MSU, IEEE Transections on Nuclear Science, NS26 (1979) 2078.